Techno-Economic and Life Cycle Assessments of Aqueous Phase Reforming for the Energetic Valorization of Winery Wastewaters

(Article begins on next page)

08 May 2026

Article

Techno-Economic and Life Cycle Assessments of Aqueous Phase Reforming for the Energetic Valorization of Winery Wastewaters

Giulia Farnocchia [1,*], Carlos E. Gómez-Camacho [2], Giuseppe Pipitone [1,*], Roland Hischier [2], Raffaele Pirone [1] and Samir Bensaid [1]

1 Department of Applied Science and Technology, Politecnico di Torino, Corso Duca degli Abruzzi 24, 10129 Turin, Italy; raffaele.pirone@polito.it (R.P.); samir.bensaid@polito.it (S.B.)

2 Technology and Society Laboratory (TSL), Swiss Federal Laboratories for Materials Science and Technology, Empa, Lerchenfeldstrasse 5, 9014 St. Gallen, Switzerland; carlos.gomez@empa.ch (C.E.G.-C.); roland.hischier@empa.ch (R.H.)

* Correspondence: giulia.farnocchia@polito.it (G.F.); giuseppe.pipitone@polito.it (G.P.)

Abstract

Globally, winery wastewaters (WWWs) are estimated to account for about 62.5 billion L annually (2021), with COD levels up to 300,000 mg O_2/L primarily attributed to residual ethanol, posing serious environmental concerns. Conventional treatments are effective in COD removal, but they often miss opportunities for energy recovery and resource valorization. This study investigates the aqueous phase reforming (APR) of ethanol-rich wastewater as an alternative treatment for both COD reduction and energy generation. Two scenarios were assessed: electricity and heat cogeneration (S1) and hydrogen production (S2). Process simulations in Aspen Plus® V14, based on lab-scale APR data, provided upscaled material and energy flows for techno-economic analysis, life cycle assessment, and energy sustainability analysis of a 2.5 m³/h plant. At 75% ethanol conversion, the minimum selling price (MSP) was USD0.80/kWh with a carbon footprint of 0.08 kg CO_2-eq/kWh for S1 and USD7.00/kg with 2.57 kg CO_2-eq/kg H_2 for S2. Interestingly, S1 revealed a non-linear trade-off between APR performance and energy integration, with higher ethanol conversion leading to a higher electricity selling price because of the increased heat reactor duty. In both cases, the main contributors to global warming potential (GWP) were platinum extraction/recovery and residual COD treatment. Both scenarios achieved a positive energy balance, with an energy return on investment (EROI) of 1.57 for S1 and 2.71 for S2. This study demonstrates the potential of APR as a strategy for self-sufficient energy valorization and additional revenue generation in wine-producing regions.

Keywords: aqueous phase reforming; energy recovery; techno-economic assessment; life cycle assessment; hydrogen production; winery wastewater valorization

1. Introduction

In response to the urgent climate goals set by international agreements, starting from the Paris Agreement [1] and being reinforced by the European Green Deal [2], a rapid and widespread transition toward renewable energy sources is imperative to achieve net-zero CO_2 emissions by 2050. Simultaneously, the growing global population, projected to reach 9.8 billion by 2050 [3], drives increasing water demand, making universal access to water and sanitation crucial.

Efficient wastewaters treatment plays a significant role not only in improving water resource management but also in reducing greenhouse gas emissions and recovering

valuable products and energy [4–6]. It is estimated that in 2010, emissions from municipal wastewaters treatment reached approximately 0.77 Gt of CO_2-equivalent (CO_2eq), accounting for around 1.6% of total anthropogenic GHG emissions [7], with an estimated increase up to 84 million t CO_2 by 2030 [6]. To address these challenges, implementing low-emission technologies is essential.

In this context, aqueous phase reforming (APR) emerges as a potential solution to meet both objectives [8–10]: on one hand, achieving COD abatement and, on the other, producing a H_2-rich combustible gas stream suitable either for cogeneration or as a specific energy vector, i.e., hydrogen. APR is a mild thermo-catalytic process, first studied by Dumesic et al. [11,12], designed to convert biomass-derived oxygenated hydrocarbons into hydrogen using a heterogeneous catalyst, according to the following stoichiometric relation:

$$C_nH_{2y}O_n \ + \ nH_2O \ \leftrightarrow \ nCO_2 \ + \ (y+n)H_2 \tag{1}$$
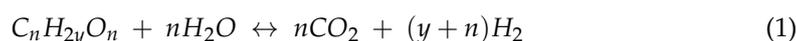
The above equation is the sum of the carbohydrates reforming with a C:O ratio of 1:1, such as methanol, ethylene glycol, glycerol, etc. (2) and the water gas shift reaction (WGS) (3), to reduce CO content and promote additional H_2 formation [13].

$$C_nH_{2y}O_n \ \leftrightarrow nCO + H_2 \tag{2}$$

$$CO + H_2O \leftrightarrow CO_2 + H_2 \tag{3}$$

The APR reaction typically occurs at temperatures between 200 °C and 280 °C and under autogenous pressure (15–65 bar). H_2 production by APR represents a milder alternative compared to traditional thermochemical processes, such as steam reforming and gasification, which operate at temperatures from 600 to 1000 °C [14,15]. Numerous studies have investigated single model compounds, suggesting that short-chain alcohols are highly selective towards hydrogen production [16]. Specifically, experimental studies on ethanol APR have been performed [17–19], showing up to 99% conversion and a molar gas composition of up to 55 vol% H_2. Several studies on APR have highlighted that wastewaters from breweries [20,21], lignocellulosic biomass [8,10,22,23], starch-based processes [24], and cheese whey [25] could serve as potential feedstock for energetic valorization strategies, as they contain compounds that are not fully oxidized and thus retain chemical energy, which could still be exploited.

An innovative approach involves using bioethanol commonly found in wastewaters from wineries, breweries, and distilleries [26,27]. In 2021, global wine production was estimated at approximately 25 billion L [28]. Considering that winery wastewater (WWW) generation ranges from 1 to 4 L per liter of wine, this corresponds to an average estimated 62.5 billion L of WWW produced worldwide in the same year [29]. Moreover, WWW contains high COD values ranging from 800 to 300,000 mg O_2/L [30], with ethanol alone contributing up to 70 wt.% of the total organic carbon (TOC). Other components include organic acids (e.g., acetic acid and tartaric acid), soluble sugars (e.g., glucose and fructose), high molecular weight compounds (e.g., lignin and tannins), inorganic salts, and traces of heavy metals [30]. Conventionally, ethanol remaining in WWW is recovered at distilleries for purification into high-alcohol-grade beverages (e.g., grappa and brandy). The remaining effluent is then treated using conventional biological processes [31]. However, ethanol concentration in wastewater varies greatly with the processing stage, winery size, and product diversity [29], posing challenges for distillation-based recovery [32]. Additionally, distilleries themselves have a significant environmental impact; it was estimated that the production of 1 hectoliter of pure alcohol in a distillery generates approximately 900 kg of CO_2-equivalent emissions [33]. Alternative biological processes for WWW treatment include constructed wetlands and microbial fuel cells (MFCs). Wetlands can achieve up to 88% COD removal, while MFCs reach around 42% but they offer the added benefit of

energy recovery [34]. Conventional biological treatments, widely used for winery effluents, typically achieve 80–97% COD removal [35,36] yet often fail to meet discharge limits and do not aim to recover energy. In addition, they have long retention times (24–48 h) and require large storage volumes, lowering overall process efficiency [37].

Even with research efforts, APR development remains largely confined to laboratory-scale studies. This highlights the need for a comprehensive evaluation of the process, both from the economic and environmental point of view, via techno-economic analysis (TEA) and life cycle assessment (LCA), respectively [38–41]. Specifically, TEA helps identify the major cost drivers of the process, offering opportunities for optimization and guiding research efforts toward more economically viable configurations. In parallel, LCA extends the assessment by providing a system-level overview of the environmental impacts associated with the technology, allowing the identification and prioritization of environmental hotspots that then could be addressed to ensure the overall sustainability. Additionally, to complement the techno-economic and environmental assessments, an energy sustainability analysis (ESA) can provide a structured method to evaluate the ability of an energy-producing process to provide surplus useful energy to the society after accounting for the energy required for its operation and supporting activities, including material and energy supply, decommissioning, and waste treatment [42].

Therefore, the present work aims to advance the understanding of wastewater-based APR by evaluating the feasibility of implementing this technology at an industrial scale for ethanol-rich wastewater from an energetic, economic, and environmental perspective. While the combined use of TEA and its integration with LCA has already been applied to other APR feedstocks, the novelty of this study lies in extending the approach to winery wastewater. In fact, with ethanol as the primary organic component, it could be potentially converted into different energetic carriers (electricity/hydrogen) according to previous published works [17,18]. Furthermore, the integration with ESA, scarcely employed in the APR field, broadens the analysis towards the long-term energetic sustainability of the technology. In this work, winery wastewater was simplified to an ethanol-rich aqueous solution. This choice was motivated by two reasons. First, our aim was to derive preliminary insights under ideal conditions, following a "boundary-limit" approach: if the sustainability indicators are not satisfied even in this simplified case, more complex scenarios would be even less feasible. Second, based on our previous experience with complex APR feedstocks [16,25], ethanol can be considered a reasonable proxy, as other components (e.g., acetic acid and sugars) either play a minor role or introduce additional trade-offs, such as promoting hydrogen formation while accelerating catalyst deactivation. This assumption, while simplifying, allows us to highlight the main sustainability challenges and bottlenecks while setting the stage for future studies on more realistic wastewater streams. The scaled-up process is subdivided into three main sections: pretreatment; the APR reaction section; and downstream processing. Since the APR gaseous product is a mixture of hydrogen and methane (in addition to CO_2), two downstream configurations were evaluated taking into account two possible valorization pathways: (i) an energy valorization chain, where heat and electricity are produced exploiting the calorific value of the total gas mixture and (ii) a material valorization chain, where hydrogen is sold as main product, while additional energy is obtained exploiting the methane-rich residual gas mixture. In both scenarios, energy integration strategies are adopted to improve overall energy efficiency and move toward process self-sufficiency, as observed in similar works [43]. Finally, optimized scenarios were investigated to minimize the environmental impact and to identify the key economic parameters that could enhance the profitability of the process

2. Materials and Methods

This study adopts a multi-stage methodological framework to evaluate the energetic performance, technical feasibility, and sustainability of APR applied to ethanol-rich wastewater. Firstly, the feedstock was characterized, and subsequently, lab-scale APR tests were performed to determine product distribution and referential yields. Results from bench-scale experiments served as input values for process simulations conducted at an upscaled flow rate of 2.5 m^3/h. Specifically, two energy recovery strategies were explored:

- Scenario 1 (S1): The produced gas phase is entirely valorized through cogeneration, supplying both the thermal and electrical demands of the plant. The surplus electricity is sold.
- Scenario 2 (S2): Hydrogen is first separated and purified via pressure swing adsorption (PSA) for external sale, while the remaining combustible gases are used in cogeneration to meet the plant's energy needs. Any excess electricity is also sold.

ESA was applied to quantify the net energy balance (Section 2.4), followed by TEA (Section 2.5) and LCA (Section 2.6) to evaluate the process in view of their economic and environmental performances. Finally, a sensitivity analysis was performed to evaluate how optimized scenarios affected energetic, economic, and environmental parameters. These include increasing ethanol conversion to 95% (referred to as S1–95 and S2–95) and/or modifying accordingly process configurations. Specifically, an additional flash unit was introduced in S1 (S1–95+), while S2 was enhanced with both an additional flash and a compressor (S2–95+), aiming to enhance both energy recovery and wastewater treatment efficiency. Table S1, in Supporting Information, summarizes the different scenarios analyzed and their corresponding abbreviations.

2.1. Wastewater Characterization

A comprehensive investigation was conducted on the characteristics of WWW to evaluate its properties and the issues related to its disposal. This included direct discussions with winery producers and wastewater treatment operators, as well as the collection of real wastewater samples from a local winery (Frescobaldi, Florence, Italy). The sample was analyzed by high-performance liquid chromatography (HPLC) (Prominence Shimadzu, Kyoto, Japan) equipped with a refractive index detector (RID-10A Shimadzu, Kyoto, Japan) and a 300 mm·7.8 mm ROA-Organic Acid H$^+$ (8%) column (Rezex Phenomenex, Torrance, CA, USA). The mobile phase consisted of 5 mM H$_2$SO$_4$ in water, operated at a flow rate of 0.7 mL/min and a column temperature of 50 °C. Total organic carbon (TOC) was measured using a TOC-VCSH analyzer (Shimadzu, Kyoto, Japan) equipped with a non-dispersive infrared detector. The main component was found to be ethanol, with final concentrations ranging from 1 to 5 wt.%, in line with literature references [31,35]. Table S2 reports the primary compounds identified. For the sake of this preliminary assessment, only ethanol APR was considered for the process simulation, given its predominance in the wastewater.

2.2. Bench-Scale APR Tests

APR tests were performed in duplicates in a continuous-flow fixed-bed reactor (Microactivity Effi, Micromeritics, Norcross, GA, USA) made of SS316 stainless steel (ID: 9.1 mm, length: 305 mm), loaded with 1.0 g of 5.0 wt.% Pt/C catalyst. The reactor was heated at 270 °C, measured through a thermocouple in the catalyst bed, while 100 °C was set in the external oven. A 5 wt.% ethanol aqueous solution was fed at 1 mL/min using a Gilson HPLC pump, corresponding to a residence time of ~3 min.

Ethanol conversion was monitored through HPLC analysis of the liquid phase (using the same equipment described in Section 2.1). External calibration curves were prepared to ensure that the concentrations of all compounds remained within the calibrated range.

The gas composition was analyzed using a micro-gas chromatograph (SRA Instruments, Milano, Italy) equipped with two columns (Agilent Technologies, Santa Clara, CA, USA) and a thermal conductivity detector (TCD). A Molsieve 5A column (Agilent Technologies, Santa Clara, CA, USA) was used for the detection of H_2, O_2, N_2, CH_4, and CO with Ar as the carrier. The column operating temperature was 85 °C with a head pressure of 28 psi, while the injection temperature was 100 °C. The second column, a PoraPLOT U column, was employed for the separation of CO_2, C_2H_4, C_2H_6, C_3H_{10}, and H_2O, using He as the carrier. The operating temperature was set at 80 °C and a head pressure of 30 psi, while the injection temperature was equal to 90 °C. The concentration of the specific component in the gas phase was measured following an external calibration methodology.

2.3. Process Simulation

These bench-scale experimental results were then used for simulating an upscaled process at a reference plant capacity of 2.5 m³/h of ethanol-rich wastewater, typical for medium to large production wineries [44], operating during 8 months for 24 h/day. Regarding the composition of winery wastewater, the concentrations of glucose and fructose were far below the ~1 wt.% C threshold identified in our previous work for significant humin formation [25]. Under such diluted conditions, the theoretical hydrogen contribution from these sugars would be negligible compared to that from ethanol while also not expected to negatively affect catalyst stability. Acetic acid, although frequently reported in winery effluents, was not detected in our sample; moreover, our earlier studies have shown that it behaves essentially as an inert species in APR, with no detrimental impact on hydrogen yield or catalyst durability [16]. The process flows were optimized through simulations conducted on AspenONE Performance Engineering (Aspen Plus® V14.0.1, Burlington, VT, USA), enabling a detailed analysis of related mass and energy flows. The Peng–Robinson (PR) equation of state and the Non-Random Two-Liquid (NRTL) activity coefficient model were chosen for the simulation, based on the characteristics of the systems [45]. Both scenarios share the same upstream configuration aimed at meeting the specific APR input requirements. As shown in the process flow diagrams for each scenario (Figures 1 and 2), since WWW typically contains a 0.5–1.5 wt.% solids fraction [46,47], the feedstock is firstly stored (STR in Figure 1) and allowed to clarify and remove suspended solids (clarifier, CLR). The clarified inflow water stream is subsequently pressurized at 80 bar using a high-pressure pump (PMP1), and it is heated up using two different heat exchangers. In the first one (HE1), the liquid stream recovers the thermal energy from the APR reactor effluent. This step raises the temperature of the feed up to 250 °C. In the second stage, a second heater (HE2) is used to provide the additional thermal duty required in order to reach the final operating temperature of 270 °C prior to the APR reactor (REAC). The reactor is modeled assuming isothermal plug flow conditions at 270 °C and 80 bar in both scenarios, using a rstoic reactor in the process simulation software. A baseline conversion rate of 75% for ethanol was set based on the experimental data. Subsequent to the APR reactor, the two scenarios differ then in their downstream configurations.
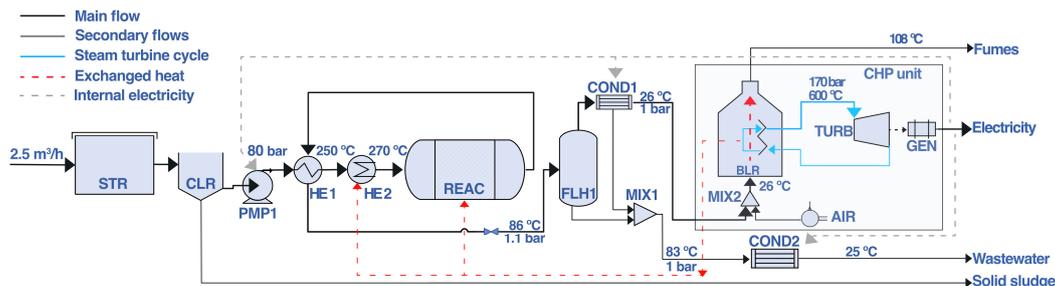
Figure 1. Scenario 1—Process flow diagram for the cogeneration of electricity and heat. Thermal energy, shown in red, is entirely used to meet the plant's internal heat demands, while net electricity, after covering the plant's electrical needs (shown in grey), exits the system. Abbreviation: STR: storage tank. CLR: clarifier. PUMP1: pump1. HE1–HE2: heat exchanger 1–2. REAC: APR reactor. FLH1: flash 1. COND1–COND2: condenser1–2. MIX1–MIX2: mixer1–2. BLR: blower. TURB: turbine. GEN: generator.
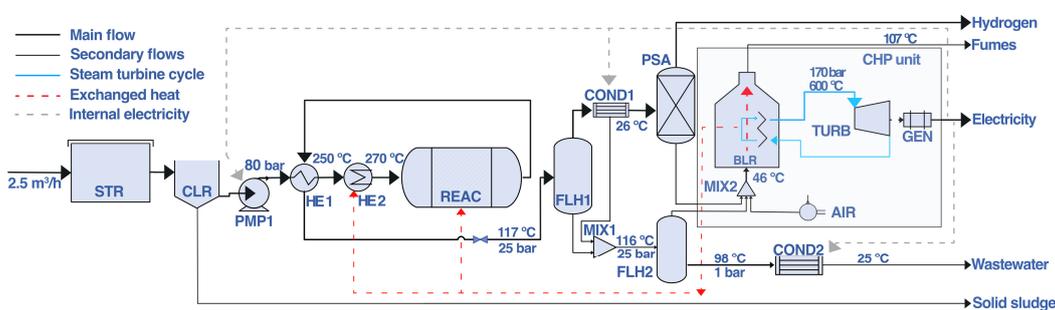

Figure 2. Scenario 2—Process flow diagram for hydrogen separation and purification. Heat integration (red dashed lines) and internal electricity use (grey dashed lines) are illustrated. Thermal energy is entirely used to meet the plant's heating demands, while the net electricity, after covering internal requirements, is exported for external sale. Abbreviation: STR: storage tank. CLR: clarifier. PUMP1: pump1. HE1–HE2: heat exchanger 1–2. REAC: APR reactor. FLH1–FLH2: flash 1–2. COND1–COND2: condenser1–2. MIX1–MIX2: mixer1–2. BLR: blower. TURB: turbine. GEN: generator.

Figure 1 illustrates the process flow diagram for S1, showing the energy recovery configuration aimed at achieving plant energy self-sufficiency and maximizing electricity export to the grid.

In S1, the effluent from the APR reactor after exchanging part of its heat with the first HE1 is expanded to 1.1 bar to maximize the phase separation, resulting in a temperature drop from 118 °C to 86 °C. An L-G separation is performed, then in the subsequent flash unit (FLH1). The resulting gas phase (primarily composed of H_2, CH_4, and CO_2, see Section 3.1.2) is directed to a condenser (COND1) and cooled to 36 °C to remove residual steam using cooling water. The dry gas stream then enters the combined heat and power (CHP) unit which generates high-pressure steam, serving a dual purpose: A fraction is used to satisfy the thermal requirements of the process, including feed preheating (HE2) and heat reactor duty, while the excess is expanded through a steam turbine (TURB) to generate electricity (electrical efficiency = 36%). The CHP is shown in a simplified form in the process flow diagram, while a more detailed explanation and representation (and modeling in the process simulation software) is provided in Section 3.1.3 and Figure S1, accordingly. Lastly, the liquid phase separated in the flash unit is further cooled to room temperature and exits the system as wastewater with a reduced COD content. Depending on the configuration adopted (see Section 3.4), at this point, the wastewater may undergo additional treatment.

In Figure 2, the S2 process flow diagram is shown, where the focus shifts to the production of hydrogen (the detailed process simulation flowsheet can be found in Figure S5). In this configuration, the reactor effluent is firstly depressurized to 25 bar, matching the PSA operating pressure, before entering a flash separator, for a first L-G separation. The resulting gas stream is then further cooled down to ambient temperature before entering the additional PSA unit for the hydrogen purification. Furthermore, the liquid stream from the first flash undergoes a second flash separation, exploiting the pressure drop from 25 to 1 bar to further enhance ethanol removal from the liquid phase and reduce the liquid COD content while contributing to the cogeneration. In fact, the tail gas from the PSA, together with the recovered ethanol from the second flash, is sent to the CHP unit. As in S1, the CHP thermal and electric outputs are firstly evaluated for the feasibility to match the internal energy demand of the plant. The surplus electricity is externally sold, contributing to the plant's revenues.

2.4. Energy Sustainability Analysis (ESA)

To evaluate the energy efficiency and sustainability of the process, an ESA was carried out. Mass and energy flows were derived from process simulations, which were extrapolated to assess the energy performance of both scenarios. The energy flows that characterize the process and are identified in the analysis are defined as follows:

- Available energy, $E_{available}$, MJ: This refers to the energy content of the material inputs to the process. In this study, ethanol is the main available source of energy, and its lower heating value (LHV) is used to quantify the input energy. Although not directly used in the ESA calculation, $E_{available}$ is reported to establish a consistent reference point across both scenarios.
- Produced energy, $E_{produced}$, MJ: This represents the total energy output generated by the system. For S1, it is calculated as the sum of the thermal and electrical energy produced. For S2, it includes the same contributions, along with the intrinsic chemical energy (i.e., LHV) of the recovered hydrogen.
- Direct energy, E_{direct}, MJ: This includes the energy directly required to operate the plant, such as the thermal energy needed by the APR reactor and heat exchangers, as well as the electrical duties required by pumps and compressors.
- Indirect energy, $E_{indirect}$, MJ: This accounts for all additional energy contributions associated with each component considered in the analysis, including catalyst synthesis, equipment manufacturing, and waste treatments.

Figure 3 illustrates the schematic energy flows involved in the processes under investigation.
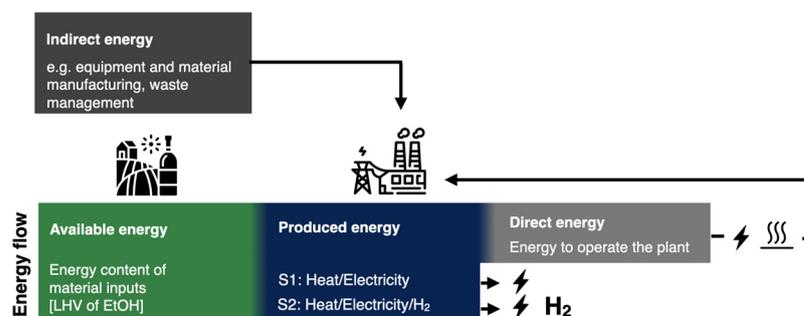

Figure 3. Energy flow diagram of the process. The available energy—ethanol content in winery wastewater—is identical in both scenarios. In S1, heat and electricity are cogenerated, with surplus electricity sold. In S2, hydrogen is recovered and sold first, while residual energy supports cogeneration and additional electricity sales.

All energy flows were normalized for the ESA to one hour of plant operation and are expressed in MJ/h. The key indicators employed in the ESA include the Energy Sustainability Index (ESI) and the Energy Return on Investment (EROI) [42]. The ESI provides preliminary insight into the short-term self-sufficiency of a technology from an energetic point of view. It is calculated according to the following equation (Equation (4)), which represents a simplified form of the original formulation reported by Gómez-Camacho [48]:

$$ESI = \frac{E_{produced}}{E_{direct}} \tag{4}$$

An ESI value greater than 1 is indicative of an energy self-sustaining system at the short-term level since there is a surplus—during operation—of produced energy compared to the required energy by the plant. The EROI, on the other hand, aims at evaluating the long-term energy sustainability by considering also the indirect energy that society must divert for the plant construction/demolition and the required chemicals/materials. The EROI metric is calculated as the ratio between the net energy output and the indirect energy, as expressed in Equation (5):

$$EROI = \frac{E_{produced} - E_{direct}}{2 * (E_{indirect})} \tag{5}$$

To calculate the indirect energy, the cumulative energy demand (CED) metric from the CED LCA methodology is used, following the inventory compilation as suggested in the work from Ruggeri et al. [49], here conservatively approximated as multiplying the CED by two. This correction for the EROI allows to estimate the total indirect energy, as it accounts for maintenance, decommissioning, plant construction, and the amortization of the next plant, in order to guarantee that the energy surplus, after direct energy expenditures, is sufficient not only to repay the construction/decommissioning of the current facility but also to support the development of the next generation of infrastructure.

2.5. Techno-Economic Analysis (TEA)

Cost estimations were carried out following mainly the methodology proposed by Towler and Sinnott [50], commonly applied in techno-economic evaluations of industrial processes, including APR processes from different sources [51,52]. The economic assumptions adopted in this work are referenced to the European context, integrating country-specific data where available. In particular, labor costs were taken from Italy, wastewater treatment costs from Spain, and interest rates from the European Central Bank.

All reported costs have been adjusted to monetary 2024 values and are expressed in USD_{2024} (from hereafter, USD for simplicity). The total cost of production (TCOP, USD/y) on an annual basis was estimated according to the following equation:

$$TCOP = VCOP + FCOP + ACC \tag{6}$$

VCOP are the variable costs of production (USD/y) and refer to costs that depend on the annual plant's production rate. Regarding VCOP, it should be noted that two different COD treatment costs are considered, as wastewaters with COD levels above 500 ppm typically must be treated in a dedicated facility, with an average cost of ~USD1.05 per kg of COD removed [53]. In contrast, wastewaters with COD below this threshold can be discharged into public sewage systems (e.g., in Italy, in compliance with Legislative Decree 152/2006 [54] and the EU Urban Wastewater Treatment Directive [55]). In this case, disposal costs are significantly lower and usually depend on discharged volume. For the estimation, a cost of ~USD0.53/m^3 was adopted, based on a study of municipal wastewater treatment plants in Europe (Jaén, Spain [56]). Catalyst cost was calculated assuming the use of 5 wt.% Pt/C with a 1-month lifespan and 99% recycling. Only 1 wt.% fresh catalyst replacement per month was considered in the cost estimation, a conservative assumption compared to

the common TEA practice of omitting catalyst cost entirely [51], or assuming longer catalyst lifespan as reported in similar works [52]. Detailed assumed costs are reported in Table 1.

FCOP refers to the annual fixed costs of production (USD/y), and it includes those costs that are independent of the production rate. Main cost drivers are listed in Table 1, generally estimated as fixed percentages based on the process's technological readiness, novelty, and other relevant economic parameters [50].

The ACC (USD/y) term corresponds to the annualized capital charge, and it is defined in Equation (9) as follows:

$$ACC = FCI \times CRF \tag{7}$$

FCI refers to the fixed capital investment (USD), and consists of four main components: (i) ISBL—inside battery limits—representing the cost of all the core plant equipment, including installation costs; (ii) OSBL—outside battery limits—which covers costs related to additional infrastructure and supporting facilities required for the plant construction; (iii) engineering costs, which account for project design and consulting services; and (iv) contingency charges, which account for unexpected costs that may arise, especially in first-time plant construction as in this case.

CRF is the capital recovery factor (-), which annualizes the fixed capital investment over the expected equipment lifetime (*n*, years) and discount rate (*i*, %), and it is expressed as follows:

$$CRF = \frac{i\,(1+1)^n}{(1+1)^n - 1} \tag{8}$$

where the discount rate (*i*) accounts for the real interest rate, adjusted to reflect inflation rates (ca. 0.7%/year) [57]. To clearly present the economic structure of the system under study, Table 1 summarizes the items and corresponding values considered in the VCOP, FCOP, and ACC calculations.

Table 1. Cost parameters and unit costs adopted for the TEA analysis, including raw materials, operating, and capital-related costs (VCOP, FCOP, and ACC).

Category	Parameter	Value	Unit	Reference
Raw materials	Fresh Pt	30.70	USD/g	[58]
	Fresh activated carbon	2.75	USD/kg	[59]
	Solids transport	0.02 *	USD/kg	[60]
	COD treatment > 500 ppm	1.05	USD/kg	[53]
	COD treatment < 500 ppm	0.53	USD/m^3	[56]
Fixed operation costs	Labor	24 588.0	USD/year/shift position	[61]
	Supervision	25.0	% labor	[50]
	Maintenance	4.0	% ISBL	[50]
	Insurance	1.5	% ISBL + OSBL	[50]
	Overhead charges	50.0	% labor + supervision	[50]
	Land rent	1.5	% ISBL + OSBL	[50]
Economic parameters in ACC	ISBL	-	-	[50,62]
	OSBL	40.0	% ISBL	[50]
	Engineering cost	25.0	% ISBL + OSBL	[50]
	Contingency	10.0	% ISBL + OSBL	[50]
	CRF	6.5	%	[50]
	Plant life	20.0	years	assumed
	Nominal interest rate	3.4	%	[63]
	Inflation	0.7	%	[57]
	Real interest rate	2.6	%	calculated

* Assumptions: 50 km distance with a 2000 kg capacity diesel truck, diesel efficiency: 3.5 km/L, driver wage of 20 USD/h.

For ISBL cost estimation, equipment sizes and capacities were first determined based on the mass and energy flows obtained from the scaled-up process simulation. These flows were used to define the technical specifications of each unit operation required for the equipment purchase cost calculations. Details on the equipment specifications and the capacity units adopted are provided in Sections 3.1.4 and 3.2. Equipment purchase costs were estimated using two different approaches, depending on data availability. Specifically, two databases were employed: the carbon capture usage and storage (CCUS) database [62] and the Towler and Sinnott database, while the costs for the CHP unit and the APR reactor were derived from literature works [51,64]. The two cost estimation equations adopted from these sources are as follows [50,62]:

$$C_{eq.} = a + (b * S^n) \tag{9}$$

$$C_{eq.} = C_{min} + \left(\frac{S}{S_{min}}\right)^n \tag{10}$$

where a and b are cost constants, S is the size or capacity of the equipment (e.g., flow rate, power, and volume), n is the size-scaling exponent, and C_{min} is the cost of the equipment at a reference minimum size (S_{min}). Once the purchase costs were determined, four correction factors were applied to obtain the final (or bare module) equipment costs: the installation factors from Wroth [65], the material factor [50], the pressure factor from Allen [65], and a cost updated to the 2024 Chemical Engineering Plant Cost Index (CEPCI) [66]. All factors are summarized in Table S3.

The economic viability was assessed by determining the minimum selling price (MSP) of electricity (in USD/kWh) and hydrogen (in USD/kg H_2). The MSP was calculated as the ratio of the annualized cost of each scenario (i.e., USDTCOP/year) to the annual expected production of electricity (i.e., kWh/year) in S1 and hydrogen (i.e., kgH_2/year) in S2. In S2, the annual surplus electricity generated from the combustion of tail gases after H_2 separation was assumed to be sold at the current market price (USD0.36/kWh) [67], and the corresponding annual revenue was subtracted from the TCOP/year.

2.6. Life Cycle Assessment (LCA)

The LCA was carried out in order to evaluate, in a prospective manner, the potential environmental impacts associated with the application of APR to WWW. The impacts were benchmarked against similar technologies focused on the same type of energy vector produced from each scenario. For S1, electricity was compared with that generated from different national energy mixes, as well as with key renewable technologies, including photovoltaic, geothermal, and hydropower. For S2, hydrogen production was compared with conventional steam methane reforming and water electrolysis.

The assessment was carried out following the International Organization for Standardization (ISO) 14040–14044 standards [68,69]. The system boundary includes all relevant processes from cradle to grave for the treatment of residual WWW, as shown in Figure S2. The considered life cycle stages are (i) the supply of raw material and the construction of the facility (i.e., using the proxy dataset of "chemical plant construction, organics unit"), (ii) the operative phase (for which the process simulations data is used), and (iii) the end-of-life (including decommissioning and materials post-use). For a proportional allocation of the "*chemical plant construction, organics unit*", the quota was prorated based on plant's capacity according to each scenario. The scaling approach was based primarily on S2, where the construction quota was allocated proportionally to the kg of H_2 produced, using as reference the quota adopted in the dataset for "steam reforming", since the scaling was straightforwardly given the same functional unit (i.e., 1 kg of hydrogen produced). In S1, the construction share was distributed proportionally to the treated wastewater volume,

using the volume treated in S2 (0.36 m^3) as a reference, and scaling it accordingly for S1, 1.29·10^{-2} m^3. This method ensures consistency across scenarios while reflecting their different functional outputs (1 kWh of electricity in S1 and 1 kg of hydrogen in S2). Specific assumptions and estimates are reported in Table S4.

The background model used the *ecoinvent v3.9.1 cut-off* life cycle inventory database [70] due to its comprehensive coverage and wide applicability, and the LCA calculations were performed using the *brightway2* framework in python, via the *Activity Browser* (AB) interface [71], chosen for its ease of use, flexibility, and open-source nature. The life cycle impact assessment (LCIA) step was carried out using the Environmental Footprint (EF) v3.1 no LT method, with particular attention to the global warming potential (GWP100) category. Regarding CO_2 emissions, both direct and indirect emissions are accounted for. The characterization factors of the EF method consider non-fossil direct CO_2 emissions as 0, while fossil emissions are accounted for as +1. The summarized cornerstone of the LCA of the present study is reported in Table 2.

Table 2. Summary of the cornerstones for the present LCA study.

LCA Step	Details
I—Goal and scope definition	Evaluate the environmental footprint of ethanol APR from WWW for electricity (S1) and/or H_2 (S2) production through attributional LCA Benchmarking against alternative technologies Functional units (FUs): 1 kWh of electricity (S1), 1 kg H_2 (S2)
II—Inventory analysis	Boundaries of analysis: cradle-to-gate approach, including raw material extraction, end-of-life treatment of the infrastructure and of the WWW. Foreground: based on data provided from the (upscaled) process simulations, basic equipment sizing for materials Background: *ecoinvent 3.9*, system model: *cutoff* Calculation implementation: python *brightway2* framework in *Activity Browser*
III—Impact assessment	Selected indicators from Environmental Footprint (EF) methodology v3.1 no LT were used for impact assessment, GWP100 (with +1/0 CFs for fossil/non fossil carbon), and total aggregated single score impact (i.e., through EF normalization)
IV—Interpretation	Compare the LCA results for each scenario and benchmark against alternative technologies

Note: Italics are used only for proper nouns such as software and database names.

Furthermore, a comparative assessment was performed between S1 and S2 based on overall environmental impacts, using a single-score approach following the EF methodology [72]. To enable a fair comparison from an energy perspective, hydrogen production was converted into its energy equivalent using the LHV of hydrogen. Single-score results were calculated by first normalizing the midpoint impact category results using global normalization factors [73] and then applying the official weighting factors proposed by Sala et al. [74] in accordance with the EF v3.1 no LT method. The final single score for each scenario was obtained by summing the weighted normalized values across all impact categories, thus providing a referential metric for directly comparing the overall environmental burden of the two configurations.

3. Results and Discussion

3.1. Process Simulations for Material and Energy Balances

3.1.1. Upstream Configuration

In the upstream configuration, common to both scenarios, a 78 m^3 storage tank was selected, sized for one day of operation plus a 30% margin, based on a wastewater input flow of 2.5 m^3/h. The subsequent clarifier was designed with a surface overflow rate (SOR) of 0.3 m^3/h·m^2, chosen as a conservative value compared to typical SORs for biologically
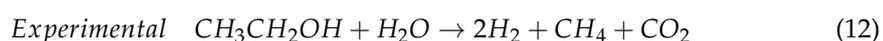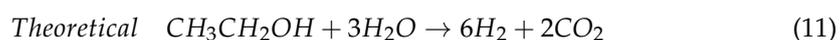
treated municipal wastewater [75], in order to maximize the settling efficiency of particles of all sizes, including degradation products of leaves and other organic residues from wine production, present in winery wastewater (here referred as solids). The clarified effluent is firstly pressured and then heated at APR operating conditions. The common upstream equipment and its characteristics are reported in Table 3.

Table 3. Lists of common upstream equipment for Scenario 1 and Scenario 2, reported with design specifications.

Unit	Sizing Reference	Specification
Storage tank	Volume: 78.0 m^3	One day inflow + 30% of capacity
Clarifier	Flow rate: 2.5 m^3/h	3 h retention time, SOR: 0.3 m^3/h·m^2 Volume: 8.0 m^3
High-pressure pump	Power rating: 19.0 kW	Discharge pressure: 5.00 bar Flow rate: 0.7 L/s
Heat exchanger 1 (HE1)	Surface: 13.0 m^2	Shell and tube, net energy exchanged: 741.0 kW U: 1250.0 W/m^2·K, fouling effect considered
Heat exchanger 2 (HE2)	Surface: 3.0 m^2	Shell and tube, net energy exchanged: 84.0 kW U: 2750.0 W/m^2·K, fouling effect considered
APR reactor	Input flow: 2525.0 kg/h	Volume: 0.14 m^3, 3.3 min retention time Catalyst loading: 70.0 kg

3.1.2. The APR Reactor

Under the studied conditions, the theoretical APR stoichiometry for ethanol—(i.e., 1 mol EtOH/6 mol H$_2$) (4)—was not fully evinced. Instead, the observed product composition followed a different experimental stoichiometry, with roughly 2 mol H$_2$ and 1 mol CH$_4$ produced per mol of converted ethanol. The observed conversion trend and main gas product composition over time are reported in Figure S3. Under the selected operating conditions, ethanol conversion reached approximately 75%. The two stoichiometries are outlined below:

$$\textit{Theoretical} \quad CH_3CH_2OH + 3H_2O \rightarrow 6H_2 + 2CO_2 \tag{11}$$

$$\textit{Experimental} \quad CH_3CH_2OH + H_2O \rightarrow 2H_2 + CH_4 + CO_2 \tag{12}$$

The observed stoichiometry from the experimental bench-scale tests was used for the subsequent calculations and process simulations to ensure a conservative estimate compared to the ideal performance. These values served as the basis for the preliminary mass and energy balance evaluation, supporting the process simulations and the economic and environmental assessments. The Aspen Plus process simulation flowsheets, along with the corresponding mass flows and operating conditions (pressure and temperature) of each stream, are reported in Figures S4 and S5 and Tables S5 and S6 for Scenarios 1 and 2, respectively. The APR reactor operating pressure was established based on sensitivity analyses, scanning conditions between 60 and 110 bar, and observing the resulting steam fraction together with the APR duty. These values were chosen on one side to ensure a minimum overpressure with respect to the vapor pressure at the set temperature (ca. 55 bar at 270 °C) to guarantee the liquid phase and, on the other side, to avoid the use of higher pressures, which may be challenging for the materials used and the design of the reactor itself. At lower APR pressure conditions, an increase in energy demand was observed, consistent with findings from other studies [76]. This increase in the reactor's thermal duty is associated with greater vapor fraction formation, as illustrated in Figure 4. The reactor duty is primarily driven by the latent heat of water vaporization (ΔH_{vap} = 1604.5 kJ/kgH$_2$O at 55 bar), along with the endothermic nature of the ethanol

APR reaction (ΔH°_{rxn}= +95.1 kJ/molEtOH), resulting in additional heat required during hydrogen production. Therefore, increasing the reactor's pressure reduces the vapor fraction in the output, which consequently lowers the reactor duty, because less energy is lost due to vaporization (see Figure 4). To some extent, operating at high pressure would be ideal to minimize this effect by further reducing the vapor fraction. However, excessively high reactor pressures were observed to reduce gas productivity and lower overall APR performance [77]. The simulations showed that above 75 bar, the vapor fraction is already significantly reduced—falling below 30%—and begins to level off, indicating the onset of a plateau. This suggests that a favorable trade-off can be achieved between operating pressure and vaporization extent, optimizing process efficiency under high-pressure conditions. Therefore, 80 bar was selected as the operating pressure to minimize energy consumption while maintaining satisfactory process performance.
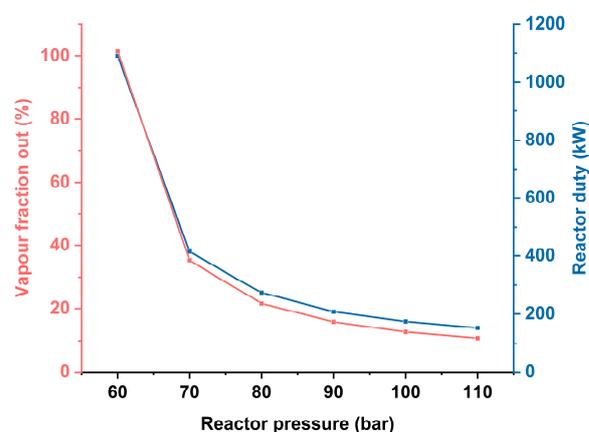

Figure 4. Influence of APR operating pressure on the thermal reactor duty and vapor fraction in the outlet stream.

Besides the same upstream processing and core reaction section (APR), the downstream phase is distinct among the two scenarios, with each equipment designed according to the specific requirements and products.

3.1.3. Downstream Scenario 1—Electricity Production

For S1, the downstream processing included a flash stage to separate the gas and liquid phases. According to Towler and Sinnott, the inlet gas velocity should be below 30 m/s; under the studied conditions, a velocity of 0.05 m/s was calculated using gas and liquid densities from the Aspen simulation. A retention time of 10 min was selected to ensure complete settling of liquid droplets, resulting in a minimum vessel diameter of 1.3 m [78]. The final flash volume was set at 0.55 m^3, including a 25% safety margin above the minimum, as suggested by Towler and Sinnot [78]. The separated gas phase was further cooled to 36 °C and mixed with a slightly pressurized (1.1 bar) air stream containing 10% excess oxygen relative to the stoichiometric requirement for the combustion of the APR gas products. The mixture was assumed to be combusted in a boiler, generating a high-temperature flue gas stream at 1665 °C, starting from an initial temperature of 26 °C, with a *Cp* of 1.5 kJ/kg·K, estimated from process simulations. Adiabatic conditions were assumed, and a conservative temperature value was adopted by excluding the heat released through water condensation. This calculated temperature is consistent with typical flue gas temperatures from hydrocarbon combustion [79,80]. This flue gas was used to produce high-pressure steam for cogeneration. Specifically, a total thermal power of 319 kW and electric power of 195 kW are produced by the CHP. The recovered heat could potentially cover the APR reactor duty at 270 °C (235 kW) and the secondary heat exchanger, HE2

(84 kW), used for the final feed preheating from 250 to 270 °C. After covering the total 319 kW of thermal power required by the process, the remaining heat is used to generate high-pressure steam (HPS) at 170 bar and 620 °C, with a mass flow rate of c. 550 kg/h, through a Rankine cycle, where the flue gas flows counter-currently through four successive heat exchangers (see Figure S1): (1) a superheater, which raises the steam temperature from 352 °C to 620 °C; (2) a reboiler, providing the latent heat of vaporization at 170 bar; and (3) two economizers. The first economizer heats liquid water at 170 bar from ambient conditions to 275 °C (729 kg/h flow directed to process units), while the second raises the temperature of the remaining water flow (550 kg/h) from 275 °C to 352 °C. Finally, the HPS expands in a steam turbine, where its pressure is reduced to 0.1 bar, enabling a maximum electricity generation of 195 kW. The exhaust gases are released from the system at temperatures between 100 and 110 °C to prevent condensation and any related operational issues. After subtracting the internal electricity consumption—mainly due to pumps and compressors (30 kW)— the net surplus electricity (165 kW) remains available to be exported to the grid. In this configuration, the wastewater leaving the plant must be sent to wastewater treatment, as its COD level (1268 ppm) remains above the limits set by national regulations for discharge into the sewage system (500 ppm) or surface waters (150 ppm) [54]. To reduce the residual COD below 150 ppm, further modifications should be implemented, as discussed in Sections 3.4.1 and 3.4.2.

3.1.4. Downstream Scenario 2—Hydrogen Production

The S2 configuration shares certain similarities with S1; however, the downstream process configuration is specifically adapted for hydrogen production. After the heat recovery in HE1, the stream is expanded to 25 bar before entering Flash 1. At this point, a first gas–liquid separation occurred. The gas phase output of Flash 1 was at 117 °C, and it was then cooled to 26 °C by a condenser before entering the PSA unit. The PSA unit was modeled to operate at 25 bar and 26 °C, consistent with literature references, which reported hydrogen purities of 99% and recovery efficiencies around 85% for feed streams containing approximately 10 mol% H_2 [81]. From an energy perspective, the PSA energy duty was assumed negligible by exploiting the high pressure of the APR output stream since compression is typically the main energy-intensive step [82].

The liquid phase exiting Flash 1 was mixed with the liquid separated at the condenser (before the PSA unit), and it was fed to a second flash, where the pressure drops to 1 bar. This caused the temperature to drop from 117 °C to 98 °C and enabled the recovery of 89 wt% of the residual ethanol in the liquid phase, originating from unconverted ethanol in the APR effluent. This step effectively reduced the COD of the remaining water, which was subsequently cooled to room temperature and, if needed—depending on the configuration, if implemented or not (see Sections 3.4.1 and 3.4.2)—sent to a wastewater treatment plant. The generated gas phase, along with the PSA tail gases, was directed to the boiler for cogeneration. Specifically, treating 2.5 m^3/h of winery wastewater yielded a total thermal power of 319 kW and 115 kW of gross electricity. Due to the additional hydrogen separation step in S2, the overall LHV of the gas stream sent to the CHP system decreased by 26% compared to S1, resulting in a flue gas temperature of approximately 1462 °C. Nonetheless, following the methodology previously described, the entire thermal output was used to meet the plant's internal heat requirements, while 87 kW of net electricity remained available for external sale after covering internal demands. The specifications for the downstream equipment employed in the two scenarios are detailed in Table 4. The flowsheets, along with the stream tables (phase, temperature, and pressure) obtained from Aspen for S1 and S2, are presented in Figures S4 and S5 and Tables S5 and S6, respectively.

Table 4. Downstream equipment specification for Scenarios 1 and 2, with equipment capacities in bold used for cost estimation.

Equipment	Scenario 1	Scenario 2
Flash 1	P: 1.1 bar Tin: 118 °C Tout: 86 °C Duty: 0 kW RT: 10 min Settling velocity: 0.1 m/s **Vol: 0.55 m^3**	P: 25 bar Tin: 118 °C Tout: 117 °C Duty: 0 kW RT: 10 min Settling velocity: 0.1 m/s **Vol: 0.49 m^3**
Condenser 1	Double pipe Net heat exchanged: 114 kW **Area: 6.08 m^2** U: 1000 W/m^2·K	Double pipe Net heat exchanged: 20 kW **Area: 1.12 m^2** U: 1000 W/m^2·K
PSA	-	P: 25 bar T: 26 °C 99% H_2 purity 85% H_2 recovery 7 kg/h H_2
Flash 2	-	P: 1 bar T: 97.5 °C Duty: −9.15 kW RT: 10 min Settling velocity: 0.1 m/s **Vol: 0.55 m^3**
Condenser 2	Plate and frame Net heat exchanged: 171 kW **Area: 13 m^2** U: 1150 W/m^2·K	Plate and frame Net heat exchanged: 210 kW **Area: 16 m^2** U: 1150 W/m^2·K
Air blower	**Flow rate: 1230 kg/h** Power rating: 2.8 kW P: 1.1 bar Isentropic compression	**Flow rate: 952 kg/h** Power rating: 2.2 kW P: 1.1 bar Isentropic compression
CHP (Boiler + turbine + generator)	Fuel LHV: 956 kW Fumes T: 1665 °C **Electricity capacity: 195 kW** 0.6 wt.% water content	Fuel LHV: 712 kW Fumes T: 1462 °C **Electricity capacity: 115 kW** 6 wt.% water content
	η_{el}: 20% Thermal capacity: 319 kW $\eta_{thermic}$: 33% $\eta_{isentropic}$: 85% $\eta_{mechanical}$: 100% Discharge pressure: 0.1 bar 6% heat loss (LHV)	η_{el}: 16% Thermal capacity: 319 kW $\eta_{thermic}$: 44% $\eta_{isentropic}$: 85% $\eta_{mechanical}$: 100% Discharge pressure: 0.1 bar 6% heat loss (LHV)
Pump CHP 1	Discharge pressure: 170 bar ΔP: 110 bar Flow rate: 0.2 L/s **Power rating: 3.4 kW** η: 95%	Discharge pressure: 170 bar ΔP: 110 bar Flow rate: 0.2 L/s **Power rating: 3.4 kW** η: 95%
Pump CHP 2	Discharge pressure: 170 bar ΔP: 171 bar Flow rate: 0.15 L/s **Power rating: 2.8 kW** η: 95%	Discharge pressure: 170 bar ΔP: 171 bar Flow rate: 0.09 L/s **Power rating: 1.9 kW** η: 95%

Table 4. *Cont.*

Equipment	Scenario 1	Scenario 2
Economizer CHP 1	Double pipe Net heat exchanged: 170 kW **Area: 1.95 m²** U: 769 W/m²·K	Double pipe Net heat exchanged: 100 kW **Area: 1.82 m²** U: 769 W/m²·K
Economizer CHP 2	Double pipe Net heat exchanged: 215 kW **Area: 0.83 m²** U: 769 W/m²·K	Double pipe Net heat exchanged: 177 kW **Area: 1.10 m²** U: 769 W/m²·K
Reboiler CHP	Double pipe Net heat exchanged: 298 kW **Area: 0.5 m²** U: 769 W/m²·K	Double pipe Net heat exchanged: 244 kW **Area: 0.5 m²** U: 769 W/m²·K
Heater CHP	Double pipe Net heat exchanged: 137 kW **Area: 0.17 m²** U: 769 W/m²·K	Double pipe Net heat exchanged: 82 kW **Area: 0.12 m²** U: 769 W/m²·K
Cooling water	25–40 °C Total plant flow rate: 36 m³/h	25–40 °C Total plant flow rate: 27 m³/h

Note: Bold text indicates the equipment specifications adopted as cost-scaling parameters.

3.2. Energy Sustainability Assessment (ESA) Results

The energy sustainability of S1 and S2 was assessed using the ESA methodology described in Section 2.4. The most relevant energy flows for the scenarios under study, expressed in MJ/h and the ESI and EROI terms for 75 and 95% conversion of each scenario, are summarized in Table 5. Scenarios assuming 95% ethanol conversion were evaluated for both S1 and S2 (S1–95 and S2–95) to examine how enhanced conversion influences the overall energy performance of the process.

Table 5. Detailed energy flows included for the ESA evaluation as previously shown in Figure 3.

Scenario	S1	S1–95	S2	S2–95
Ethanol conversion (%)	75	95	75	95
Available energy (MJ/h)	3384	3384	3384	3384
Produced energy (MJ/h)	1850	1990	2409	2725
Direct energy (MJ/h)	1254	1442	1247	1436
Indirect energy (MJ/h)	380	346	428	371
Net energy (MJ/h)	596	549	1162	1288
ESI	1.48	1.38	1.93	1.90
EROI	1.57	1.59	2.71	3.47

Starting from the same available energy content in ethanol, the two scenarios lead to different outputs in terms of produced energy and quality types. At 75% ethanol conversion, S2 delivers 2409 MJ/h, corresponding to a 30% increase compared to S1. Differences in the produced energy also account for the different thermodynamic efficiencies for each quality conversion. The difference between S1 and S2 slightly increases at 95% ethanol conversion, where the energy output of S2 is 36% higher than S1. Despite these differences in the produced energy, the direct energy requirements for plant operability remain similar across scenarios at similar conversion levels. However, a 15% increase in direct energy consumption is observed at higher ethanol conversion rates (95%), primarily due to the intensified extent of the APR reaction. This results in greater vaporization effects

(see Section 3.1.2), which in turn increases the energy duty of the APR reactor. In contrast, indirect energy consumption (associated with materials supply, catalysts, infrastructure construction/dismantling, and waste treatments) behaves inversely. Increasing ethanol conversion results in a 9% decrease in indirect energy demand for S1 and a 13% reduction for S2. This trend reflects improved energy process efficiency, enabled by higher productivity and enhanced COD removal. Together with platinum supply burdens, these factors represent the most impactful contributors to the total indirect energy invested.

Regarding the energy metrics, all ESI values are above unity, indicating that both configurations can be considered energy sustainable in the short term (i.e., able to cover their direct energy inputs and provide surplus energy in the evaluated quality forms). In both S1 and S2, the ESI undergoes a minimal decrease with increasing conversion. This could be counterintuitive, but it is explained mainly by the higher thermal duty of the APR reactor at higher ethanol conversion, leading to a reduction in the net produced energy from 195 kWh to 182 kWh. Further discussion on how reactor thermal duty is linked to the net electricity sent to the grid is reported in Section 3.1.3. Since the ESI is directly influenced by the plant's net energy output, these additional energy requirements (and reduced output) also lead to a slight decline in short-term energetic sustainability. These limited variations in ESI passing from 75% to 95% conversion highlight the importance of improving the APR reactor duty and optimizing pressure conditions, thereby improving reaction kinetics using advanced catalysts capable of lowering the activation energy of the reforming reactions or enabling similar APR performances at lower temperatures.

In terms of long-term energy sustainability, EROI values confirm a positive energy return for each scenario, albeit more energy profitable for S2. When increasing the conversion to 95%, S2 resulted in EROI rising to 3.47, a gain of over 30%, while for S1, no significant changes were observed. These differences arise primarily from the quality of the produced energy: Hydrogen in S2 is credited with its full calorific value (LHV), whereas electricity in S1 inherently includes losses due to thermodynamics. Although both systems produce similar syngas compositions (mainly H_2 and CH_4), the final energy quality and recovery pathway (including downstream configurations) ultimately drive the divergence in net energy returns.

Alternative studies on H_2-producing technologies have also adopted the ESA methodology [42]. In particular, steam methane reforming (SMR) and two-stage anaerobic digestion (TSAD) reported ESI values of 3.63 and 3.00 and EROI values of 2.47 and 2.24, respectively. Comparing them with S2, we can observe an ESI around 2-fold lower than SMR and 1.6-fold lower than TSAD, but its EROI exceeds that of SMR by 10% and TSAD by 21%. This suggests that although the technology may exhibit higher direct energy consumption during operation compared to the produced one, it ultimately reduces the indirect energy required over the long term, resulting in a higher EROI. The obtained ESI and EROI values, although relatively low compared to other energy-producing processes, remain at least above 1 (but are consistent in the range of energy recovery processes). Overall, the obtained metrics suggest that the process could theoretically cover its own direct/indirect energy needs, even with surplus useful energy that can be employed for societal purposes in both the short and long term. However, their values being close to 1 highlight the narrow margin of the APR for energy recovery. While these values theoretically indicate that energy sustainability could be attainable, the correct operation of the process is crucial to achieve it. In particular, given that the EROI values approach unity (e.g., EROI $\approx$ 1.90 depending on the scenario), the system's tolerance for inefficiencies or operational deviations is rather low. Small disruptions—such as reduced conversion efficiency, suboptimal heat integration, or increased auxiliaries energy demands—could easily drive the EROI below 1, rendering the system energetically unsustainable. Therefore, precise control of key parameters, including

reactor temperature, pressure, and feedstock composition, as well as reliable heat recovery and integration systems, is essential to ensure that the process consistently yields a net positive energy output and contributes meaningfully to long-term energy sustainability.

3.3. Techno-Economic Assessment (TEA) Results

Minimum Selling Prices

TCOP for the two scenarios was estimated at USD14.9 M and USD14.16 M, respectively, for S1 and S2. These values were annualized over a 20-year plant lifetime, resulting in annualized costs of USD823 k/year for S1 and USD805 k/year for S2. As illustrated in Figures 5 and 6, VCOP accounts for only ~4% of annualized TCOP in S1, compared to 7% in S2. The dominant VCOP component is COD treatment, which in S1 amounts to USD18 k/year—over 53% lower than in S2—and represents 57% of S1's VCOP. In contrast, COD treatment in S2 rises to USD38 k/year, accounting for 77% of VCOP (see Figure 6). The higher COD treatment cost in S2 stems primarily from its process configuration. Since the PSA unit operates at 25 bar, the first flash separator in S2 experiences a lower pressure drop compared to S1 (i.e., 1.1 bar pressure drop), limiting ethanol separation to only 50%. In contrast, S1 achieves 98% ethanol recovery in the first flash. As a result, a second flash is required in S2 to increase total ethanol recovery up to 90%.

Despite this improvement, the liquid effluent in S2 still contains a higher residual COD, driving up treatment costs and underscoring the strong dependency of COD treatment costs on incomplete ethanol conversion.

As explored in Section 3.4.1, enhancing APR performance to reach 95% ethanol conversion in both scenarios could significantly reduce these costs—by as much as 60%. Building on this, Section 3.4.2 examines how the integration of additional equipment could further lower COD levels while also influencing the MSP. Finally, the broader economic implications of adopting APR as an alternative to conventional wastewater treatment are discussed in Section 3.4.3, with a focus on the potential for avoided treatment costs.
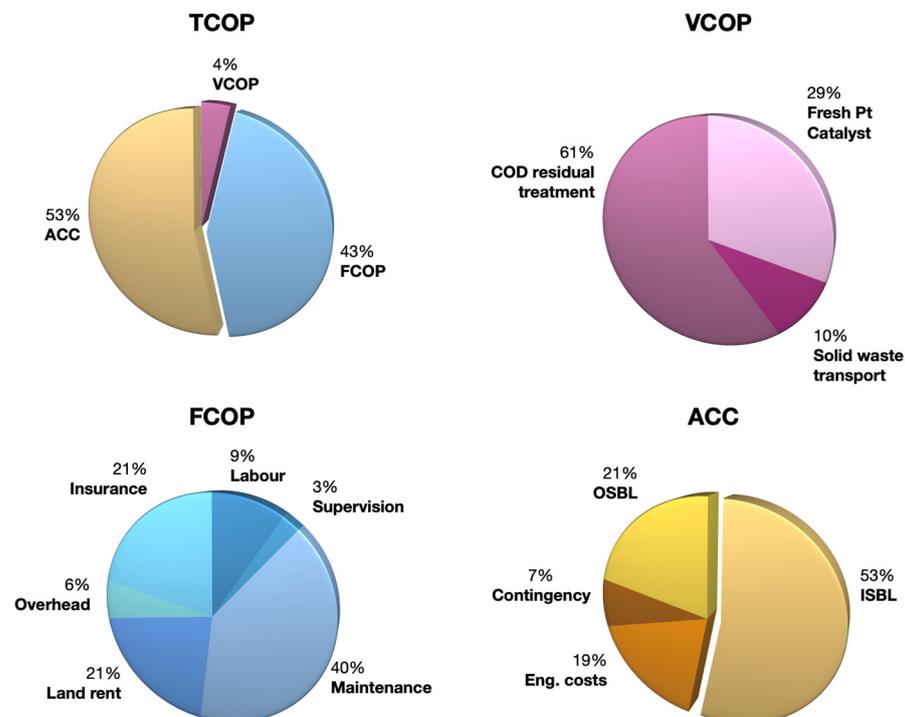

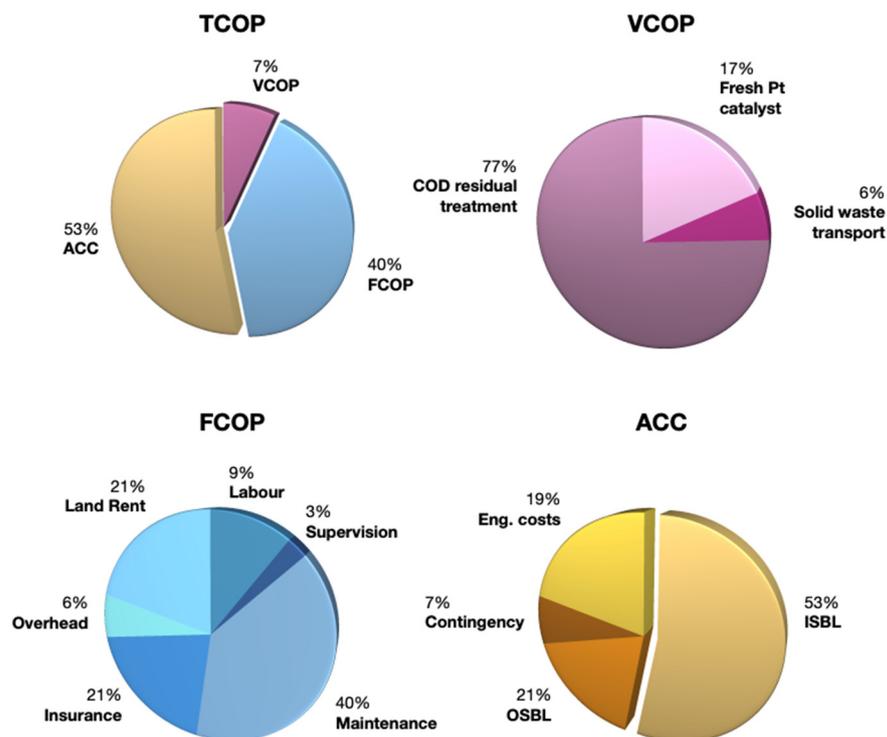**Figure 5.** Cost breakdown of the APR-based system under Scenario 1.

Figure 6. Cost breakdown of the APR-based system under Scenario 2.

Both scenarios exhibit low VCOP due to their self-sufficient operation, which eliminates utility costs. Moreover, the feedstock—WWW—is a waste stream, resulting in no associated feedstock expenses. In some cases, wastewaters represent a revenue for those facilities that must treat them (see Section 3.4.3). All remaining VCOP components are equivalent between the two cases. FCOP represents 43% and 40% of annualized TCOP in S1 and S2, respectively. As observed in similar studies on APR of glycerol [51], the largest share of FCOP in both scenarios is attributable to equipment maintenance (40%), followed by land rent and insurance.

Within the third cost term, ACC, the main contributor for both scenarios is the ISBL component, whose breakdown is illustrated in Figure 7 (6a for S1, 6b for S2). In both S1 and S2, the CHP unit is the most expensive component, accounting for 37% of ISBL in S1 (USD1.3 M) and 27% in S2 (USD901 k). The higher CHP cost in S1 is linked to the greater required generation capacity in S1, given that CHP cost scales with electric capacity [83,84].
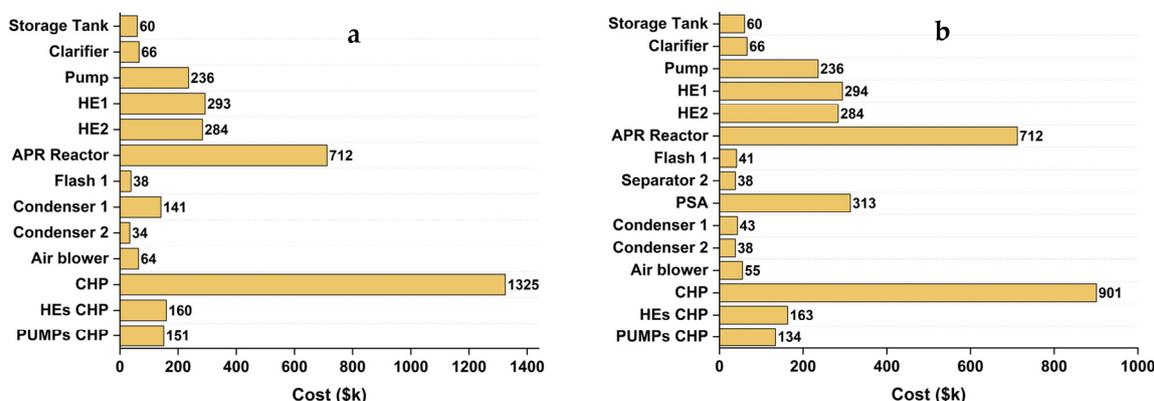

Figure 7. Breakdown of Inside Battery Limits Costs (ISBL) for the two process configurations: (**a**) Scenario 1—electricity production and (**b**) Scenario 2—hydrogen recovery.

The APR reactor is the second-highest ISBL item, representing 20% of ISBL in S1 and 21% in S2, with comparable costs for both scenarios. Stainless steel was selected as the construction material for the APR reactor, and a correction factor was applied accordingly (Table S3). This choice is consistent with previous APR TEAs, and the resulting reactor costs per unit of treated feed are in line with literature values. In S2, the PSA unit constitutes the third major cost driver, representing 9% of ISBL (USD313 k/year). In contrast, in S1, the third-largest cost component is HE1, representing 8% of ISBL. A detailed list of all equipment costs—both as-purchased and after applying correction factors (see Section 2.5 and Table S3)—contributing to the ISBL is provided in Table S7.

Taking all associated costs into account, the minimum selling prices for electricity and hydrogen are estimated at USD0.86/kWh and USD15.5/kg H_2, respectively—both significantly above current market benchmarks (USD0.36/kWh for electricity [67] and USD 2–7/kg H_2 [85]). To address this gap, optimization scenarios were evaluated through sensitivity analysis for both S1 and S2.

3.4. Sensitivity Analysis

3.4.1. Ethanol Conversion Effect

To explore opportunities for cost reduction, additional scenarios were modeled in which ethanol conversion was increased from 75% to 95% in both cases (i.e., S1–95 and S2–95).

In S1–95, TCOP slightly decreased from USD824 k/year to USD811 k/year, mainly due to lower operating costs for COD removal and CHP, which scale with the electricity generated. A schematic representation of the main cost drivers is shown in Figure S6, while Table S8 specifically compares the overall energy flows for S1 and S1–95. Despite the TCOP reduction, the MSP of electricity increased from USD0.86/kWh to USD0.92/kWh, a counterintuitive result driven by several interacting factors. First, at 95% conversion, more ethanol is transformed into reaction products, resulting in a +14.5% higher LHV in the produced gas mixture (i.e., rising from 956 to 1095 kW) with an increased flue gas flow rate from combustion (from 1400 to 1533 kg/h). The recovered heat from this stream is used to generate high-pressure steam in the CHP unit. However, the higher conversion also means higher endothermic duties of reaction together with the vaporization effect, raising the APR reactor's thermal demand by 22% (from 235 kW to 287 kW). To meet this demand, a larger portion of the generated steam is diverted to the reactor (848 kg/h vs. 729 kg/h), leaving less steam available for turbine expansion and electricity generation. Consequently, net power output from the CHP unit decreases from 195 kW to 182 kW. Since the MSP is calculated as a ratio of the TCOP and energy output, the result is an increased MSP (the numerator decreases by only 1.2%, while the denominator drops by 8.0%). Since the rise in MSP at higher ethanol conversion is largely driven by the increased reactor heat duty, mainly from water vaporization, operating at higher pressure could reduce this effect by limiting vaporization, a strategy that should be explored in future work.

In summary, higher ethanol conversion improves COD removal and fuel quality but also raises internal heat demand, shifting the utilities balance, and ultimately increasing electricity production costs. Similarly, in the S2–95 case, TCOP decreased by 5%, from USD805 k/year to USD769 k/year, more than in S1–95. While modest in absolute terms, in this case, this drop translates into a substantial 20% decrease in the hydrogen MSP, from USD15.5 to USD12.5 per kg H_2. This is driven by the combined effect of (i) the lower TCOP and (ii) a marked 27% increase in annual hydrogen production (from 40.3 to 51.2 tons/year). Within TCOP, the improved COD removal efficiency (from 97.5% to 99.6%) is particularly important, as COD treatment represents a larger share of variable costs in S2 (see Figure 6). As in S1, higher ethanol conversion increased the reactor's heat demand. However, since

hydrogen is separated in S2, the energy available for electricity generation via CHP is lower, reducing the net power output from 115 kW to 87 kW (–24%). This, in turn, slightly decreases CHP-related costs, which are tied to the electricity production scale (see Figure S7 for further details). Ultimately, the higher hydrogen yields more than offset the reduction in sold electricity (and associated revenues), making S2 more positively sensitive to improved APR performance. A more detailed comparison of the energy flows underlying the different behaviors observed when increasing conversion in S1 and S2 is provided in Table S8.

3.4.2. Configuration Effect

Increasing ethanol conversion to 95% enhanced only the S2 process economics. Regarding COD removal efficiency, it improved from 97.5% to 99.6% in S2 and from 98.0% to 99.9% in S1. Despite this, the resulting COD concentrations, 357 ppm for S2 and 226 ppm for S1, still exceeded the 150 ppm regulatory limit for surface discharge, necessitating additional treatment. To meet this requirement, a revised process configuration was implemented for both scenarios by introducing an additional flash unit.

In S1–95+, COD was reduced up to 105 ppm, hence allowing direct discharge. This result was achieved because, in the first flash stage, the pressure was sharply lowered to 6 bar, unlike in S2–95, where it was maintained at 25 bar to meet PSA feed requirements. The lower pressure enabled a more efficient G-L separation, with 80% of the ethanol removed from the liquid stream, compared with 57% in scenario S2–95. In this configuration, we also assessed the effect of recompressing the gas up to 25 bars needed for PSA feeding; however, it increased the MSP due to the added equipment cost and higher internal electricity consumption, which reduced the net power exported to the grid and consequently lowered the revenues.

The MSP of electricity reached USD0.93/kWh, which is comparable to the USD0.92/kWh of the single-flash configuration at 95% conversion (S1–95). The benefit of generating a wastewater that requires no further treatment comes at a modest cost, as the MSP increases from USD0.86/kWh at 75% ethanol conversion to USD0.92/kWh at 95% conversion. This suggests the existence of a trade-off threshold between a higher COD removal and economic efficiency.

In S2+, the revised configuration includes an initial G-L separation at 6 bar (instead of 25 bar used in S1), followed by a second flash at reduced temperature prior to PSA, and a compressor to restore inlet pressure. A third flash at atmospheric pressure is applied to the liquid stream exiting the two previous separators, improving ethanol recovery and reducing the final COD to 124 ppm, thereby fully eliminating the need for external treatment. This setup lowers the hydrogen MSP by 12% compared to the base 75% conversion, although it remains 13% higher than the two-flash 95% case (USD 13.7/kg H_2), indicating a solution optimized more for COD abatement than for economic performance (see Table 6).

Table 6. Summary of key techno-economic and environmental indicators across different APR configurations for S1 and S2.

Scenario	Conversion (%)	Turbine (kWh)	APR Revenue (USD0.315/kg$_{COD}$)	COD Removal Efficiency (%)	COD (ppm)	MSP (USD/kWh, USD/kgH$_2$)
S1	75	195	0	98.8	1268	0.86
S1*	75	195	629,350	98.8	1268	0.20
S1–95	95	182	0	99.9	226	0.92
S1–95+	95	176	0	100	105	0.93
S2	75	115	0	97.5	2809	15.52

Table 6. *Cont.*

Scenario	Conversion (%)	Turbine (kWh)	APR Revenue (USD0.315/kg$_{COD}$)	COD Removal Efficiency (%)	COD (ppm)	MSP (USD/kWh, USD/kgH$_2$)
S2*	75	115	620,988	97.5	2809	4.62
S2–95	95	87	0	99.6	357	12.59
S2–95+	95	94	0	100	124	12.59

The symbols S1* and S2* indicate scenarios where COD abatement fees are included in the cost structure.

3.4.3. Economic Benefits from Avoided Wastewater Treatment Costs

To further assess the economic viability of the APR system, a hypothetical scenario was considered in which APR is implemented as an alternative wastewater treatment process with integrated energy recovery. It was assumed that, under this perspective, APR could offer competitive market prices for electricity and hydrogen, whose average price was set at USD0.20/kWh and USD4.5/kg H$_2$, respectively, based on the data reported in Section Minimum Selling Prices. To achieve such targets, the facility would need to charge a service fee of USD0.42 per kg of COD removed—representing only 40% of the average cost of conventional treatment (USD1.05/kg COD)—making it a realistic and competitive value. Under these conditions, the APR system would generate service revenues of approximately USD629 k/year for S1 and USD620 k/year for S2, which can be directly subtracted from the respective annual TCOP. By contrast, if the same quantity of COD removed by APR—i.e., 1.49 kt/year for S1 and 1.48 kt/year for S2—were treated through a conventional wastewater treatment plant, the associated annual cost would be approximately USD1.5 million for both scenarios. This corresponds to an avoided cost of about 48% when compared to the annual TCOP of APR-based treatment for S1 and S2 (see Section Minimum Selling Prices), suggesting a potentially favorable economic benefit for the APR option. If the COD service fee is increased to 50% of the conventional cost (i.e., USD0.53/kg COD), the process could potentially achieve net-positive margins, making APR an economically attractive alternative to conventional treatment. The notations S1* and S2* refer to scenarios in which COD abatement fees are incorporated into the cost structure, assuming USD0.42 per kg of COD removed (see Table 6).

3.4.4. Minimum Selling Prices Variability

A sensitivity analysis was conducted on the base configuration by varying key cost drivers (APR reactor, CHP, PSA, COD treatment, Pt loading, and plant lifetime) by ±20% and ±40% in order to identify the main drivers to MSP and understand in which direction improvements are more important for the MSP to become more competitive. Figure 8 illustrates the resulting variation in electricity price for S1, where the reference value of USD0.86/kWh is used as the baseline (zero axis). Each bar represents the difference to the reference price associated with variation in individual cost items, including capital expenditures (i.e., APR reactor, heat exchanger HE1, CHP unit, and ISBL), operating costs (i.e., COD treatment, fresh Pt supply, and VCOP), and plant lifetime.

The same sensitivity analysis was conducted for S2. The cost variables modified and their respective impact on the reference value for hydrogen, i.e., USD15.5/kg, are presented in Figure 9.
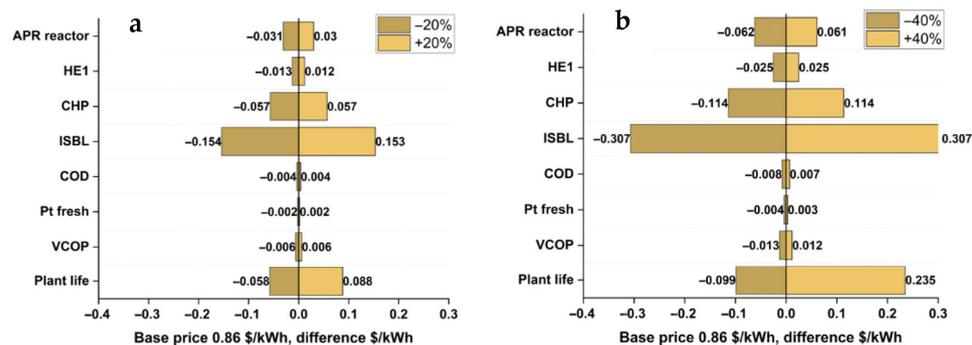
Figure 8. Variation in electricity production cost (USD/kWh) for Scenario 1 under sensitivity analysis of key techno-economic parameters, considering estimated cost fluctuations of ±20% (**a**) and ±40% (**b**). The reference electricity price is USD0.86/kWh.
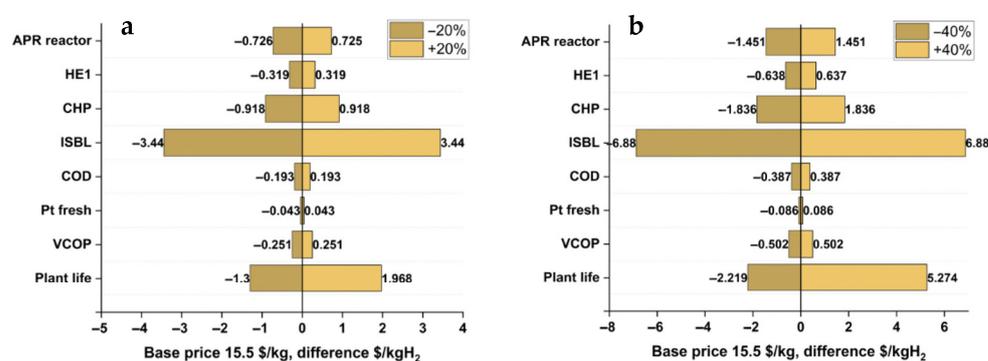

Figure 9. Variation in hydrogen production cost (USD/kg) for Scenario 2 under sensitivity analysis of key techno-economic parameters, considering estimated cost fluctuations of ±20% (**a**) and ±40% (**b**). The reference hydrogen price is USD15/kg.

It is worth noting that not all cost variables exert the same influence on the MSP. VCOP variations have only a marginal effect on both hydrogen and electricity prices. In contrast, plant lifetime proves to be a highly influential parameter in both scenarios: Extending it to 28 years (the case in which plant lifetime was varied by 40% in a positive direction) alone can reduce the electricity price to USD0.63/kWh and hydrogen production cost to USD10.2/kg. Moreover, capital investment (primarily the ISBL) was found to have the greatest influence on the reduction of MSP of the technology outputs, with CHP and APR reactor being the most impactful components within the ISBL. Electricity and hydrogen prices could decrease to as low as USD0.55/kWh and USD8.6/kg, respectively, following a 40% reduction in the ISBL cost estimate. Although lowering APR reactor costs remains challenging, the development of more active catalysts could enable shorter residence times and, in turn, smaller reactor volumes. Advancing catalyst design is therefore a key research direction, as novel formulations could be crucial to achieving economically and environmentally sustainable operation of APR plants. For the sake of example, according to Zhao et al. [86], the use of a bimetallic Ru–Pt catalyst could enable the same ethanol conversion in less than half the reaction time compared to monometallic systems. This implies that retention time could be reduced from 3.3 min to 1.65 min, potentially halving the reactor volume and reducing the reactor costs. Alternative catalyst lifespans were evaluated to account for potential faster deactivation phenomena, which may occur with real WWW (see Table S9). Reducing only the lifespan from one month to one week had a modest effect on the MSP, increasing from USD0.86/kWh to USD0.89/kWh in S1 and from USD15.40/kg to USD16.12/kg in S2 (i.e., c. 4.8–5.0% increase). However, a more pronounced rise to USD1.00/kWh (S1) and USD19.74/kg (S2) (i.e., c. 12.8–28.1% increase)

was observed when a second reactor was added in parallel to avoid weekly shutdowns for catalyst replacement. The effect of increasing the fraction of fresh Pt on the replaced catalyst per cycle from 1% (baseline) to 5%, 10%, 25%, 50%, and 100% was also assessed, showing a strong influence of fresh metal content on the final MSP. Specifically, increasing from 5% to 100% fresh Pt replacement raised the MSP from USD0.90 to USD1.76/kWh in S1 and from USD16 to USD36/kg in S2 (Figure S8). In this low-recycling rate scenario, replacing noble metal catalysts with more economic alternatives offering comparable performance could significantly reduce MSP impacts.

The ISBL cost burden could be significantly reduced if the size of the plant is increased. However, it is worth noting that the potential for exploiting economies of scale in this process is inherently limited, as the present analysis already considers wastewater volumes representative of medium-to-large wineries. Greater scale benefits could, however, be achieved within a district-scale approach, where a centralized APR facility treats effluents from multiple producers (e.g., wineries, breweries, or other industries generating ethanol-containing wastewater), which have already been suggested by the literature as possible feedstocks [8]. In such a configuration, the larger combined flow could justify higher-capacity equipment, thereby lowering specific capital costs and improving overall economic feasibility, as proposed in similar studies [87]. Furthermore, the conservative assumptions adopted in this study—such as installation factors, equipment sizing, and material choices—provide a basis for future optimization and potential MSP reductions through ISBL adjustments. For example, a contingency factor of 10% was applied in this study, consistent with the assumption of an nth plant rather than for a FOAK (first of a kind) system. This choice avoided artificially overestimating long-term sustainability indicators, particularly since the process considered here is relatively simple and closer in configuration to a (conventional) wastewater treatment plant than to a complex chemical process with multiple conversion and separation steps. To assess the robustness of this assumption, a sensitivity analysis was also performed by varying the contingency factor from 10% to 40%. The results, reported in Figure S9, show that for S1, the MSP of electricity increases from USD0.86/kWh to USD0.97/kWh, while for S2, the MSP of hydrogen rises from USD15.48/kg to USD17.70/kg.

3.5. Life Cycle Assessment (LCA) Results

The life cycle inventories and datasets for both S1 and S2 scenarios are detailed in Tables S10 and S11, while Figures 10 and 11 compare the obtained carbon footprint (GWP100) values against selected benchmark technologies. Results are expressed in kg CO_2-eq per functional unit—per kWh for S1 and per kg H_2 for S2. To contextualize the environmental performance of the APR process in terms of GWP, three reference categories were selected for direct comparison: (i) studied APR scenarios, (ii) national electricity mixes, represented by "market for electricity, medium voltage" datasets (from the background database), which account for the country-specific electricity generation mix and average distribution impacts; and (iii) electricity generated from renewable sources in Italy.

The carbon footprint is reported for four APR configurations: APR at 75% ethanol conversion with one flash (S1) and two flashes (S1+) and the same setups for 95% conversion (S1–95 and S1–95+). The lowest GWP value was achieved by the S1+ scenario, with 0.074 kg CO_2 eq./kWh, closely followed by the optimized 95% conversion scenario (S1–95+) at 0.078 kg CO_2 eq./kWh, reflecting only a 4% difference. When compared with national electricity mixes, the GWP of the best-performing APR scenario is approximately 4.8-, 5.4-, and 6.3-fold lower than the average electricity generation in Europe, Italy, and Germany, respectively. It is comparable to the French electricity mix and 2.3-fold higher than that of Switzerland. These low-carbon profiles are largely due to France's strong reliance on

nuclear power and Switzerland's predominant use of hydroelectricity, which substantially reduces their associated CO_2 emissions compared to other national mixes [88,89].
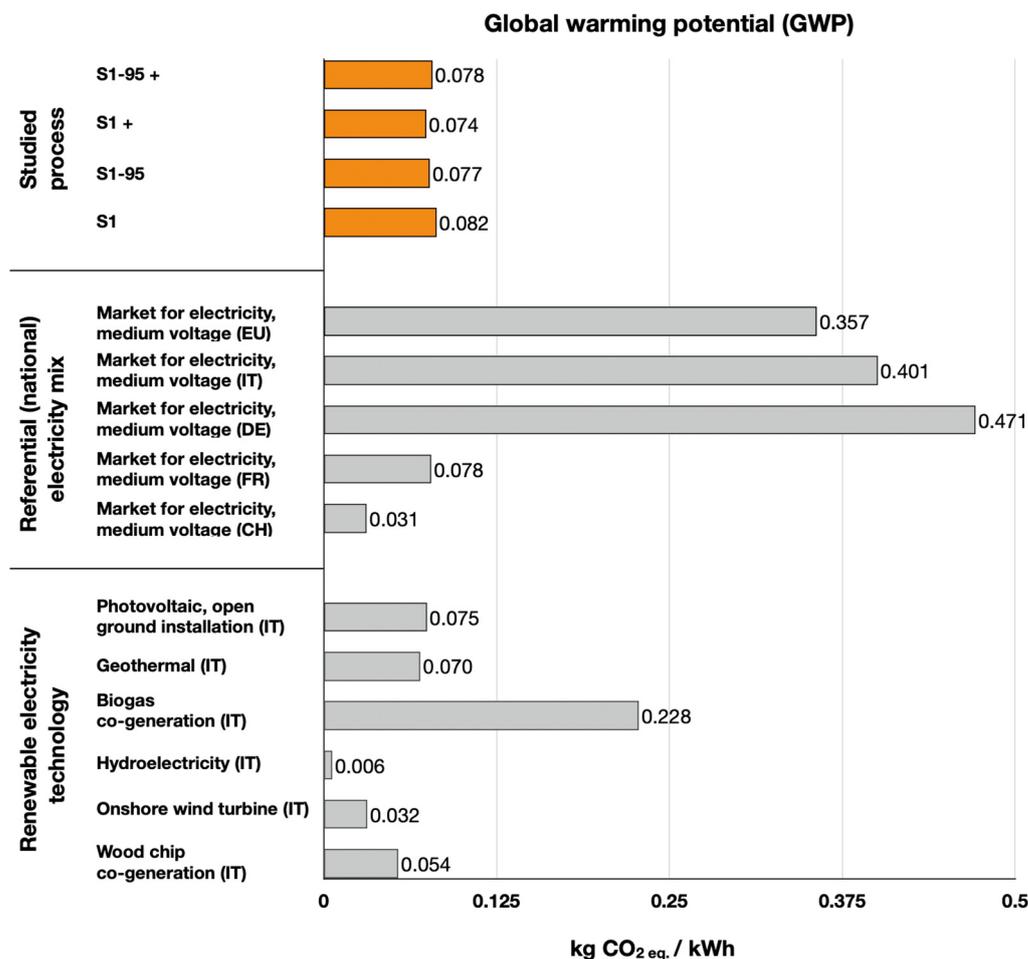

Figure 10. Comparison of APR with alternative technologies for electricity production on their GWP impact in terms of kg CO_2 eq./kWh. Referential nomenclature for APR configurations is reported in Table S1.

In relation to renewable electricity technologies in Italy, the APR process shows similar GWP to photovoltaic electricity (0.075 kg CO_2 eq./kWh), while performing 3-fold better than electricity from biogas cogeneration (0.228 kg CO_2 eq./kWh). However, APR remains less favorable than hydroelectricity, wind power, and wood chip cogeneration, all of which exhibit lower GWP values.

To evaluate the environmental performance of APR-based hydrogen production as well, three technology categories were considered for comparison in terms of GWP: (i) the studied APR scenarios, (ii) conventional hydrogen production technologies, and (iii) renewable hydrogen production technologies via water electrolysis, including both proton exchange membrane (PEM) and solid oxide electrolysis cell (SOEC) systems under different electricity supply conditions.
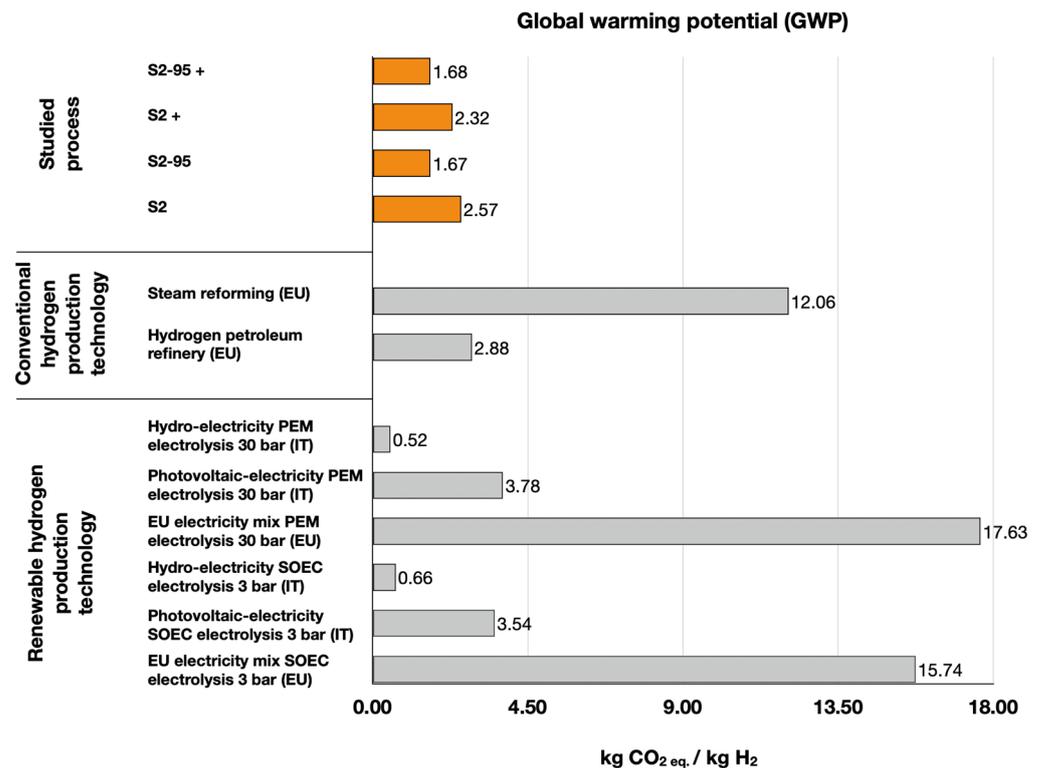
Figure 11. Comparison of APR with alternative technologies for hydrogen production on their GWP impact in terms of kg CO_2 eq./kgH_2. Referential nomenclature for APR configurations is reported in Table S1.

Among the APR scenarios, the lowest GWP was achieved with APR at 95% conversion and two flashes (S2–95), yielding 1.67 kg CO_2 eq./kg H_2, closely followed by APR at 95% conversion with three flashes (S2–95+) at 1.68 kg CO_2 eq./kg H_2. Conversely, APR at 75% conversion with two flashes (S2) showed the highest GWP, reaching 2.57 kg CO_2 eq./kg H_2. When compared with established fossil-based hydrogen production technologies, the best-performing APR scenario is approximately 7.2-fold lower in GWP than steam methane reforming (12.06 kg CO_2 eq./kg H_2) and 1.7-fold lower than hydrogen from petroleum refineries (2.88 kg CO_2 eq./kg H_2). The lower GWP is also due to the avoided burden associated with the feedstock provision for the APR process, whose production is not linked to any emissions because the environmental impacts are allocated to the primary product (wine) (i.e., no transport is considered for it). In contrast, for steam reforming and petroleum refinery processes, the feedstock includes the impacts from the extraction, processing, and transport of natural gas.

In relation to renewable hydrogen production, APR exhibits a 3.2-fold higher GWP than PEM electrolysis powered by hydroelectricity in Italy (0.52 kg CO_2 eq./kg H_2) and 2.5-fold higher than SOEC electrolysis powered by the same source (0.66 kg CO_2 eq./kg H_2). However, APR shows significantly better performance compared to electrolysis systems powered by photovoltaic electricity (3.54–3.78 kg CO_2 eq./kg H_2) and especially compared to EU grid-powered electrolysis, which could potentially reach 15.74–17.63 kg CO_2 eq./kg H_2, resulting in a 9.4–10.6-fold improvement for APR. These findings demonstrate that the source of electricity can significantly influence the GWP of electrolysis-based hydrogen production, underlining that the environmental impact of each technology is highly context dependent. The same is evident for electricity generation technologies themselves: for instance, in Switzerland—where over 90% of electricity is produced from nuclear and renewable sources—the GWP of electricity production is more than 2 times lower than

in Italy, where renewables represent only ~40% of the electricity mix [89]. Similar carbon footprints for hydrogen technologies have also been reported in previous studies [90].

Both scenarios could potentially achieve emissions reductions of approximately 80% in S1 (versus the Italian electricity mix) and 79% in S2 (versus conventional steam reforming). These lower carbon footprints can be integrated into techno-economic assessments by incorporating reduced GWP and lower externalities into cost schemes and comparative evaluations, thereby strengthening the overall value proposition (e.g., through access to carbon credits, water quality trading programs, reduced discharge fees, or eligibility for environmental subsidies). These relatively low APR impacts are mainly due to the self-sufficiency of the APR plant, which requires no external electricity or heat (and in situ carbon emissions are considered biogenic, derived from ethanol). The energy self-sufficiency of the process directly lowers environmental burdens. Furthermore, using waste as a feedstock further contributes to the reduced GWP compared to other technologies that rely on other feedstocks (including fossil sources) with higher costs linked to purity or limited availability.

A process contribution analysis was conducted to identify the main contributors to GWP under the 75% ethanol conversion scenarios with standard configurations (i.e., case with no additional flash), with cut-off values of 0.001%. Results are shown in Figure 12.
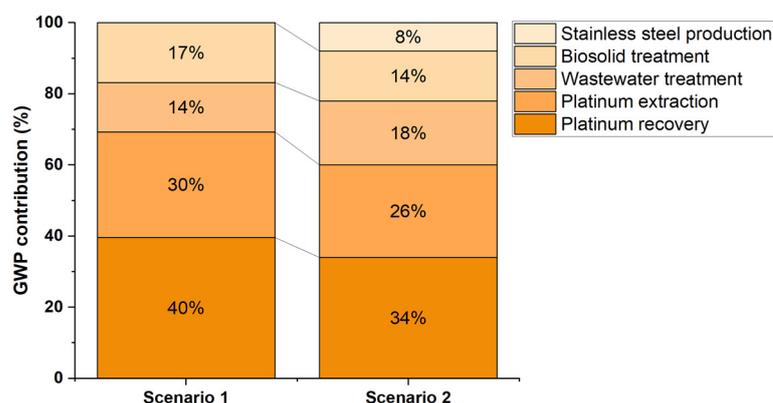

Figure 12. Main contributors to GWP are reported for S1 and S2.

The combined contributions of platinum recovery and extraction to the GWP are significant, accounting for 70% and 60% of the total impact in S1 and S2, respectively.

Although 99% of the catalyst is assumed to be recovered, the remaining 1% of fresh platinum still contributes 30% and 26% of the total GWP in S1 and S2. If the entire catalyst were sourced from primary platinum, the GWP would increase by 28-fold in S1 and 33-fold in S2. These findings underscore the high environmental burden of platinum production, even in small quantities, and highlight the critical importance of recovery strategies. Moreover, given that platinum is classified as a critical raw material by the EU, the development of more sustainable recovery processes and alternative catalysts remains a pressing priority [91]. Since the catalyst accounts for over 50% of the total GWP footprint, a sensitivity analysis on catalyst lifespan, Pt content, and Ni substitution was conducted to assess their impact. To capture potential deactivation phenomena with real wastewaters, catalyst lifespan was also varied down to 1 week, which implied installing a parallel APR reactor and resulted in a threefold GWP increase for both scenarios (for further discussion see Table S12). In addition, increasing the share of fresh Pt from 5 to 100% caused a sharp rise in the GWP, reaching 2.18 kg CO_2 eq./kWh for S1 and 60.55 kg CO_2 eq./kg H_2 for S2 (Table S13). Anyway, since Pt has a well-established recovery process, recovery rates of 95–99% can still be considered feasible, as confirmed by similar works [52,87]. This is not the case for alternative catalysts such as nickel, which is widely investigated in APR [92,93].

A key limitation for Ni and other non-precious metals is the lack of comprehensive life cycle assessments, which restricts the availability of reliable data on their supply chain impacts and prevents fair benchmarking with Pt. Addressing this gap should be a priority for future research, especially considering that Ni already shows a significantly lower environmental impact than Pt (Table S14). If Ni recovery were also found to be less impactful than Pt recovery, substituting Pt with Ni could represent a promising strategy for reducing the GWP. Based on the data currently available, we could only assess the substitution of 100% Pt with an equivalent atomic amount of Ni, without accounting for recovery and assuming identical ethanol APR performance. Under these assumptions, the GWP was reduced by approximately a factor of 72 in S1 and 56 in S2 (see Table S15).

Environmental burdens associated with wastewater and solids treatments increase proportionally with their respective volumes. This highlights the necessity of implementing efficient technologies capable of reducing the COD in wastewaters, thereby minimizing the need for additional treatment prior to environmental discharge. In S1, the adoption of an advanced configuration—achieving 95% ethanol conversion with the inclusion of an additional flash unit—eliminated the wastewater treatment requirement, hence resulting in a 40% reduction in total GWP. This improvement is primarily attributed to the mitigation of the wastewater treatment burden. In S2, the materials footprint is more significant; for example, stainless steel contributed 8% to the overall GWP, a direct result of the increased equipment requirements and associated materials used in this scenario. A Monte Carlo simulation was carried out to assess the sensitivity of the GWP results to uncertainties in the life cycle inventory, considering both the standard case (75% ethanol conversion, 1% fresh Pt) and the nickel substitution case. Assuming normally distributed variations, all input parameters were simultaneously perturbed with a standard deviation of $\pm10\%$ around their nominal values. The resulting probability distributions (Figure S10) show mean GWPs of ~0.094 kg CO_2 eq./kWh for the standard case, ~0.039 kg CO_2 eq./kWh for 100% Ni substitution in S1, and ~2.86 kg CO_2 eq./kg H_2 (standard) vs. ~1.07 kg CO_2 eq./kg H_2 (Ni) in S2. In both scenarios, the distributions are clearly separated, confirming that the reduction in GWP remains robust under considered inventory uncertainties. The mean values also fall within the most probable ranges and are consistent with the deterministic estimates. These results suggest that, if comparable catalytic performance can be achieved, replacing Pt with Ni has the potential to deliver a substantial and reliable reduction in environmental impacts.

Although GWP100 is a key metric in assessing environmental impacts, it overlooks other impact categories that may be equally important for a comprehensive evaluation. This limitation is particularly relevant, as identifying trade-offs, where improvements in one impact category may lead to deterioration in another, is a critical step in environmental analysis. To capture a more holistic picture of the process's environmental burden, this study also adopts the aggregated impact score from the EF method, which combines multiple impact categories into a single, weighted indicator. The overall environmental impacts of the two scenarios were therefore calculated by summing the weighted contributions of each EF impact category (as detailed in Section 2.6) and comparing the results on an energy-normalized basis (i.e., per kWh). The findings reveal that S1 has an overall environmental burden approximately 12% higher than S2, underscoring the importance of going beyond climate change alone when evaluating the sustainability of a system.

4. Conclusions

The present study investigated the potential implementation of APR as a treatment and valorization strategy for winery wastewaters, applying integrated energy, environmental, and economic assessment methods to two process scenarios aimed at electricity (S1) and

hydrogen (S2) production. Upscaled process simulations, based on laboratory data, suggest that processing 2.5 m^3/h of winery wastewater (ca. 5 wt. % EtOH) could generate 195 kWh in S1 and 182 kWh plus 7 kg of H$_2$ in S2. From an energy perspective, APR demonstrated strong integration potential, with the system being energetically self-sufficient in both scenarios, as confirmed by ESI values greater than 1. This energy self-sufficiency had positive implications for both the TEA and LCA. From an economic point of view, the variable cost of production (VCOP) accounted for the smallest share of the total cost of production (TCOP). In both scenarios, the main contributors to VCOP were COD treatment and (fresh) platinum usage, while the APR reactor and CHP units were the most capital-intensive components, consistent with their role as the key conversion units of the system. The resulting MSPs were USD0.86/kWh for S1 and USD15.5/kg H$_2$ for S2. Nonetheless, substantial opportunities for further MSP reduction exist. For example, a 40% reduction in ISBL costs could lower the MSP to approximately USD0.55/kWh for S1 and USD8.6/kg H$_2$ for S2—figures that, while still above current market levels, could be further improved by extending the plant lifetime from 20 to 30 years or by valorizing carbon offsets. In Scenario 1, a counterintuitive effect was also observed: as ethanol conversion increased (from 75% to 95%), the selling price of electricity also rose. This outcome stemmed from the higher thermal demand of the APR reactor at elevated conversions, which reduced the fraction of heat available for cogeneration and thus penalized electricity production, which decreased by 8%. From an environmental perspective, both scenarios could attain substantial climate benefits, with S1 reducing GWP by up to 80% compared to the Italian electricity mix, and S2 achieving a similar 80% reduction relative to conventional hydrogen production via steam methane reforming. Finally, the contribution analysis revealed that platinum extraction and catalyst treatment were the dominant drivers of environmental impact, highlighting the importance of developing durable (i.e., one month or longer), high-performance catalytic systems as a key strategy for further improving the process sustainability. Overall, APR offers a compelling circular solution that combines waste valorization, climate impact mitigation, and renewable energy generation in a single integrated approach. Future studies will focus on validating the reaction performance of APR with real winery wastewater conditions, with particular attention to long-term performance, catalyst stability, and potential process integration within existing treatment infrastructures, for the sake of assessing possible synergies and exploiting economies of scale. Furthermore, the employment of alternative catalysts will be important to evaluate techno-economic and environmental implications against Pt-based systems.

Supplementary Materials: The following supporting information can be downloaded at: https://www.mdpi.com/article/10.3390/su17177856/s1, Table S1: List of all scenarios that were evaluated by the TEA analysis and their main assumptions differences in terms of ethanol conversion and downstream configuration adopted. Table S2: Main winery wastewater organic and inorganic components detected in the sample. Figure S1: Schematic representation of the combined heat and power (CHP) unit modeled in Scenario 1. The diagram illustrates how post-APR gas products are burned with air in the boiler, and the heat from the resulting hot flue gases is exchanged with water from the water tower for electricity and heat generation. Four successive heat exchangers (I–IV) provide the heat required to meet plant thermal duties, vaporize the water, and superheat the steam to 620 °C at 170 bar for electricity production via the turbine. The reported temperatures and pressures are based on the process simulations (Aspen Plus). Table S3: Cost factors used for the calculation of the final equipment cost. Figure S2: System boundaries considered for the life cycle assessment (LCA) of the APR process for winery wastewaters valorization for Scenario 1 (a) and Scenario 2 (b). Table S4: Assumptions and estimates used for the allocation of the plant construction quota for the LCA model using the "chemical plant construction, organic" proxy from ecoinvent 3.9.1. Scaling is based on kg of H$_2$ in S2 first and from S2 as reference, while the quota for S1 was calculated based on the

treated wastewaters volumes instead. Figure S3: Experimental results of aqueous phase reforming of 5 wt.% ethanol solution in a continuous-flow fixed-bed reactor with Pt/C at 60 bar and 270 °C. Ethanol conversion (black line) is reported, together with the 95% gas products composition in vol%: H_2 (red), CH_4 (blue), and CO_2 (green). Figure S4: Scenario 1 simulation diagram extracted from Aspen plus v14. Table S5: Stream table for Scenario 1 from the Aspen plus simulation. Figure S5: Scenario 2 simulation diagram extracted from Aspen plus v14. Table S6: Stream table for Scenario 2 from the Aspen plus simulation. Table S7: Purchasing and final installed costs of each equipment item for Scenario 1 and Scenario 2. Figure S6: Bridge chart illustrating the variation in total cost of production (TCOP) for Scenario 1 as ethanol conversion increases from 75% to 95%. The bars represent the annual change in cost (USDk/year) for the main cost drivers. Green bars indicate cost reductions: COD treatment and CHP equipment decrease by USD11k/year and USD3k/year, respectively. However, these savings are partially offset by an increase of USD4k/year in other equipment costs (red bar), including the addition of Condenser 2 (COND2, see Figure S4). As a result, the overall TCOP decreases from USD823k/year to USD813k/year. Table S8: Energy balance for S1, S1-95, S2, and S2-95, with focus on those energy flows involved in the increased electricity MSP. Figure S7: Bridge chart illustrating the variation in total cost of production (TCOP) for Scenario 2 as ethanol conversion increases from 75% to 95%. The bars represent the annual change in cost (USDk/year) for the main cost drivers. Green bars indicate cost reductions: COD treatment and CHP equipment decrease by USD11k/year and USD3k/year, respectively. However, these savings are partially offset by an increase of USD4k/year in other equipment costs (red bar), including the addition of PSA. As a result, the overall TCOP decreases from USD805k/year to USD769k/year. Table S9: Impact of catalyst lifespan on the MSP for Scenario 1 (S1, USD/kWh) and Scenario 2 (S2, USD/kgH_2), respect to the baseline scenario (1 month catalyst lifespan). Figure S8: Sensitivity of the MSP for electricity (a) and hydrogen (b) to variations in the percentage of fresh Pt used relative to the recovered Pt. The base MSP for electricity is USD0.86/kWh under standard conditions, with 1% fresh Pt replacement and a catalyst lifespan of one month. The base MSP for hydrogen is USD15.4/kg under the same conditions. Figure S9: Sensitivity of the MSP for electricity (a) and hydrogen (b) to variations in the percentage of contingency (10% to 40%). Table S10: LCA dataset for Scenario 1, for 1 kWh of electricity produced from WWW APR. Table S11: LCA dataset for Scenario 2, for 1 kg H_2 produced from WWW APR. Table S12: Impact of catalyst lifespan on the global warming potential (GWP, kg CO_2 eq) for Scenario 1 (S1) and Scenario 2 (S2), respect to standard scenarios (0.08 kg CO_2 eq. per S1 and 2.57 kg CO_2 eq. for S2). Table S13: Impact of fresh platinum content in the catalysts on the global warming potential (GWP, kg CO_2 eq.) for Scenario 1 (S1) and Scenario 2 (S2), with respect to standard scenarios (0.08 kg CO_2 eq. per S1 and 2.57 kg CO_2 eq. for S2). Table S14: Global warming potential (GWP) of platinum and nickel production, expressed per functional unit (1 kg) and based on cradle-to-gate system boundaries, including the extraction and the refining processes. Table S15: Global warming potential (GWP) per functional unit (FU) for Scenarios 1 (S1: kg CO_2 eq./kWh) and 2 (S2: kg CO_2 eq./kgH_2) using 100% fresh Pt- and Ni-based catalysts. Figure S10: Monte Carlo simulation results for the global warming potential (GWP) considering ±10% standard deviation on all life cycle inventory parameters: (a) Scenario 1: GWP expressed in kg CO_2 eq./kWh in blue for the standard case (1% fresh Pt and 75% ethanol conversion), in orange for the 100% nickel substitution case; (b) Scenario 2: GWP expressed in kg CO_2 eq./kg H_2 in blue for the standard case (1% fresh Pt and 75% ethanol conversion). Each histogram shows the probability distribution of results from 200 iterations, with the vertical line indicating the mean value.

Data Availability Statement: The raw data supporting the conclusions of this article will be made available by the authors upon request.

Conflicts of Interest: The authors declare no conflicts of interest.

References

1. UNFCCC. The Paris Agreement. United Nations Framework Convention on Climate Change. 2015. Available online: https://unfccc.int/process-and-meetings/the-paris-agreement (accessed on 26 May 2025).

2. The European Green Deal. 2019. Available online: https://eur-lex.europa.eu/legal-content/EN/TXT/?uri=CELEX%3A52019DC0640 (accessed on 3 June 2025).

3. United Nations, Department of Economic and Social Affairs, Population Division. *World Urbanization Prospects: The 2018 Revision*; United Nations: New York, NY, USA, 2019.

4. Jones, E.R.; van Vliet, M.T.H.; Qadir, M.; Marc, F.P. Bierkens. Country-level and gridded estimates of wastewater production, collection, treatment and reuse. *Earth Syst. Sci. Data* **2021**, *13*, 237–254. [CrossRef]

5. Pratap, B.; Kumar, S.; Nand, S.; Azad, I.; Bharagava, R.N.; Ferreira, L.F.R.; Dutta, V. Wastewater generation and treatment by various eco-friendly technologies: Possible health hazards and further reuse for environmental safety. *Chemosphere* **2023**, *313*, 137547. [CrossRef] [PubMed]

6. Pratap, B.; Kumar, S.; Nand, S.; Azad, I.; Bharagava, R.N.; Ferreira, L.F.R.; Dutta, V. Toward Enhancing Wastewater Treatment with Resource Recovery in Integrated Assessment and Computable General Equilibrium Models. *Environ. Sci. Technol. Lett.* **2024**, *11*, 654–663. [CrossRef]

7. Tong, Y.; Liao, X.; He, Y.; Cui, X.; Wishart, M.; Zhao, F.; Liao, Y.; Zhao, Y.; Lv, X.; Xie, J.; et al. Mitigating Greenhouse Gas Emissions from Municipal Wastewater Treatment in China. *Environ. Sci. Ecotechnol.* **2023**, *20*, 100341. [CrossRef] [PubMed]

8. Zoppi, G.; Pipitone, G.; Pirone, R.; Bensaid, S. Aqueous phase reforming process for the valorization of wastewater streams: Application to different industrial scenarios. *Catal. Today* **2022**, *387*, 224–236. [CrossRef]

9. Xu, C.; Paone, E.; Rodríguez-Padrón, D.; Luque, R.; Mauriello, F. Reductive catalytic routes towards sustainable production of hydrogen, fuels and chemicals from biomass derived polyols. *Renew. Sustain. Energy Rev.* **2020**, *127*, 109852. [CrossRef]

10. González-Arias, J.; Zhang, Z.; Reina, T.R.; Odriozola, J.A. Hydrogen production by catalytic aqueous-phase reforming of waste biomass: A review. *Environ. Chem. Lett.* **2023**, *21*, 3089–3104. [CrossRef]

11. Cortright, R.D.; Davda, R.R.; Dumesic, J.A. Hydrogen from catalytic reforming of biomass-derived hydrocarbons in liquid water. *Nature* **2002**, *418*, 964–967. [CrossRef]

12. Huber, G.W.; Dumesic, J.A. An overview of aqueous-phase catalytic processes for production of hydrogen and alkanes in a biorefinery. *Catal. Today* **2006**, *111*, 119–132. [CrossRef]

13. Davda, R.R.; Shabaker, J.W.; Huber, G.W.; Cortright, R.D.; Dumesic, J.A. A review of catalytic issues and process conditions for renewable hydrogen and alkanes by aqueous-phase reform-ing of oxygenated hydrocarbons over supported metal catalysts. *Appl. Catal. B Environ.* **2005**, *56*, 171–186. [CrossRef]

14. Rosha, P.; Ali, F.M.; Ibrahim, H. Recent advances in hydrogen production through catalytic steam reforming of ethanol: Advances in catalytic de-sign. *Can. J. Chem. Eng.* **2023**, *101*, 5498–5518. [CrossRef]

15. Kumar, R.; Singh, R.; Dutta, S. Review and Outlook of Hydrogen Production through Catalytic Processes. *Energy Fuels* **2024**, *38*, 2601–2629. [CrossRef]

16. Pipitone, G.; Zoppi, G.; Ansaloni, S.; Bocchini, S.; Deorsola, F.A.; Pirone, R.; Bensaid, S. Towards the sustainable hydrogen production by catalytic conversion of C-laden biorefinery aqueous streams. *Chem. Eng. J.* **2019**, *377*, 120677. [CrossRef]

17. Nozawa, T.; Yoshida, A.; Hikichi, S.; Naito, S. Effects of Re addition upon aqueous phase reforming of ethanol over TiO2 supported Rh and Ir catalysts. *Int. J. Hydrogen Energy* **2015**, *40*, 4129–4140. [CrossRef]

18. Nozawa, T.; Mizukoshi, Y.; Yoshida, A.; Naito, S. Aqueous phase reforming of ethanol and acetic acid over TiO2 supported Ru catalysts. *Appl. Catal. B Environ.* **2014**, *146*, 221–226. [CrossRef]

19. Waheed, A.; Wang, X.; Maeda, N.; Naito, S.; Baiker, A. Surface processes occurring during aqueous phase ethanol reforming on Ru/TiO2 tracked by ATR-IR spectroscopy. *Appl. Catal. A Gen.* **2019**, *581*, 111–115. [CrossRef]

20. Oliveira, A.S.; Cordero-Lanzac, T.; Baeza, J.A.; Calvo, L.; Heras, F.; Rodriguez, J.J.; Gilarranz, M.A. Continuous aqueous phase reforming of a synthetic brewery wastewater with Pt/C and PtRe/C catalysts for biohy-drogen production. *Chemosphere* **2021**, *281*, 130885. [CrossRef]

21. Oliveira, A.S.; Baeza, J.A.; Calvo, L.; Alonso-Morales, N.; Heras, F.; Rodriguez, J.J.; Gilarranz, M.A. Production of hydrogen from brewery wastewater by aqueous phase reforming with Pt/C catalysts. *Appl. Catal. B Environ.* **2019**, *245*, 367–375. [CrossRef]

22. Li, M.; Ji, W.; Huang, C.; Si, X.; Liu, Q.; Lu, R.; Lu, T. A Review on Green Hydrogen Production by Aqueous Phase Reforming of Lignocellulose and Derivatives. *Catalysts* **2025**, *15*, 280. [CrossRef]

23. Messori, A.; Martelli, G.; Piazzi, A.; Basile, F.; De Maron, J.; Fasolini, A.; Mazzoni, R. Molecular Ruthenium Cyclopentadienone Bifunctional Catalysts for the Conversion of Sugar Platforms to Hydro-gen. *ChemPlusChem* **2023**, *88*, e202300357. [CrossRef] [PubMed]

24. Oliveira, A.S.; Baeza, J.A.; Calvo, L.; Gilarranz, M.A. Aqueous phase reforming of starch wastewater over Pt and Pt-based bimetallic catalysts for green hydrogen pro-duction. *Chem. Eng. J.* **2023**, *460*, 141770. [CrossRef]

25. Pipitone, G.; Pirone, R.; Bensaid, S. Aqueous Phase Reforming of Dairy Wastewater for Hydrogen Production: An Experimental and Energetic Assessment. *Sustainability* **2024**, *16*, 1743. [CrossRef]

26. Seluy, L.G.; Isla, M.A. A Process To Treat High-Strength Brewery Wastewater via Ethanol Recovery and Vinasse Fermentation. *Ind. Eng. Chem. Res.* **2014**, *53*, 17043–17050. [CrossRef]

27. Jorge, N.; Teixeira, A.R.; Gomes, A.; Peres, J.A.; Lucas, M.S. Winery Wastewater: Challenges and Perspectives. In Proceedings of the 4th International Electronic Conference on Applied Sciences, Online, 27 October–10 November 2023; MDPI: Basel, Switzerland, 2023; p. 267. [CrossRef]

28. International Organisation of Vine and Wine. 2024 World Wine Production Outlook—OIV First Estimates, Dijon, France, 29 November 2024. Available online: https://www.oiv.int/sites/default/files/2024-11/OIV_2024_World_Wine_Production_Outlook.pdf (accessed on 9 August 2025).

29. Miklas, V.; Touš, M.; Miklasová, M.; Máša, V.; Horňák, D. Winery Wastewater Treatment Technologies: Current Trends and Future Perspective. *Chem. Eng. Trans.* **2022**, *94*, 847–852. [CrossRef]

30. Bustamante, M.A.; Paredes, C.; Moral, R.; Moreno-Caselles, J.; Pérez-Espinosa, A.; Pérez-Murcia, M.D. Uses of winery and distillery effluents in agriculture: Characterisation of nutrient and hazardous components. *Water Sci. Technol.* **2005**, *51*, 145–151. [CrossRef]

31. Italian Republic. Law No. 238 of 12 December 2016 on the Organic Regulation of Vine Cultivation and Wine Production and Trade 2016. Available online: https://www.normattiva.it/ (accessed on 27 August 2025).

32. Howell, C.L.; Myburgh, P.A.; Lategan, E.L.; Hoffman, J.E. Seasonal Variation in Composition of Winery Wastewater in the Breede River Valley with Respect to Classical Water Quality Parameters. *S. Afr. J. Enol. Vitic.* **2016**, *37*. [CrossRef]

33. Becker, S.; Bouzdine-Chameeva, T.; Jaegler, A. The carbon neutrality principle: A case study in the French spirits sector. *J. Clean. Prod.* **2020**, *274*, 122739. [CrossRef]

34. Melchiors, E.; Freire, F.B. Winery wastewater treatment: A systematic review of traditional and emerging technologies and their efficiencies. *Environ. Process.* **2023**, *10*, 43. [CrossRef]

35. Andreottola, G.; Foladori, P.; Ziglio, G. Biological treatment of winery wastewater: An overview. *Water Sci. Technol.* **2009**, *60*, 1117–1125. [CrossRef]

36. Vlotman, D.E.; Key, D.; Bladergroen, B.J. Technological advances in winery wastewater treatment: A comprehensive review. *S. Afr. J. Enol. Vitic.* **2022**, *43*, 58–80. [CrossRef]

37. Sravan, J.S.; Matsakas, L.; Sarkar, O. Advances in biological wastewater treatment processes: Focus on low-carbon energy and resource recovery in bio-refinery context. *Bioengineering* **2024**, *11*, 281. [CrossRef]

38. Heras, F.; Justicia, J.; Baeza, J.A.; Gilarranz, M.A.; Ferro, V.R. Energy and economic analysis of alternatives for the valorization of hydrogen-rich stream produced in the aqueous phase reforming of pyrolysis bio-oil aqueous fraction. *Bioresour. Technol.* **2024**, *399*, 130572. [CrossRef]

39. Antonini, C.; Treyer, K.; Streb, A.; van der Spek, M.; Bauer, C.; Mazzotti, M. Hydrogen production from natural gas and biomethane with carbon capture and storage—A techno-environmental analysis. *Sustain. Energy Fuels.* **2020**, *4*, 2967–2986. [CrossRef]

40. Mahmud, R. Integration of Techno-Economic Analysis (TEA) and Life Cycle Assessment (LCA) for Sustainable Process Design. Ph.D. Thesis, Clemson University, Clemson, SC, USA, August 2022.

41. Giuliano, A.; Medici, A.R.; Barletta, D. Integrating Techno-Economic and Environmental Criteria in the Design and Optimization of A Full Utilization Multiproduct Lignocellulosic Biorefinery. *ACS Sustain. Chem. Eng.* **2025**, *13*, 1961–1973. [CrossRef]

42. Di Addario, M.; Luongo Malavè, A.C.; Sanfilippo, S.; Fino, D.; Ruggeri, B. Evaluation of sustainable useful index (SUI) by fuzzy approach for energy producing processes. *Chem. Eng. Res. Des.* **2016**, *107*, 153–166. [CrossRef]

43. Heras, F.; de Oliveira, A.S.; Baeza, J.A.; Calvo, L.; Ferro, V.R.; Gilarranz, M.A. Toward Sustainability of the Aqueous Phase Reforming of Wastewater: Heat Recovery and Integration. *Appl. Sci.* **2022**, *12*, 10424. [CrossRef]

44. Latessa, S.H.; Hanley, L.; Tao, W. Characteristics and practical treatment technologies of winery wastewater: A review for wastewater management at small wineries. *J. Environ. Manag.* **2023**, *342*, 118343. [CrossRef] [PubMed]

45. Neau, E.; Nicolas, C.; Jaubert, J.-N.; Mutelet, F. The generalized NRTL model associated with the Peng-Robinson equation of state to predict liquid-liquid equilibria between hydrocarbons, water and ethylene glycol. *Pol. J. Chem.* **2006**, *80*, 27–35.

46. Ioannou, L.A.; Puma, G.L.; Fatta-Kassinos, D. Treatment of winery wastewater by physicochemical, biological and advanced processes: A review. *J. Hazard. Mater.* **2015**, *286*, 343–368. [CrossRef] [PubMed]

47. Mader, A.E.; Holtman, G.A.; Welz, P.J. Treatment wetlands and phyto-technologies for remediation of winery effluent: Challenges and opportunities. *Sci. Total Environ.* **2022**, *807*, 150544. [CrossRef]

48. Gómez-Camacho, C.E.; Ruggeri, B. Energy Sustainability Analysis (ESA) of Energy-Producing Processes: A Case Study on Distributed H_2 Production. *Sustainability* **2019**, *11*, 4911. [CrossRef]

49. Ruggeri, B.; Gómez-Camacho, C.E.N. Georgescu-Roegen's production model for EROI evaluation. Case study: Electrolytic H_2 production using solar energy. *Energy Convers. Manag.* **2023**, *283*, 116915. [CrossRef]

50. Sinnott, R.; Towler, G. Costing and Project Evaluation. In *Chemical Engineering Design*; Elsevier: Amsterdam, The Netherlands, 2020; pp. 275–369. [CrossRef]

51. Khodabandehloo, M.; Larimi, A.; Khorasheh, F. Comparative process modeling and techno-economic evaluation of renewable hydrogen production by glycerol re-forming in aqueous and gaseous phase. *Energy Convers. Manag.* **2020**, *225*, 113483. [CrossRef]

52. Sladkovskiy, D.A.; Godina, L.I.; Semikin, K.V.; Sladkovskaya, E.V.; Smirnova, D.A.; Murzin, D.Y. Process design and techno-economical analysis of hydrogen production by aqueous phase reforming of sorbito. *Chem. Eng. Res. Des.* **2018**, *134*, 104–116. [CrossRef]

53. Jiménez-Benítez, A.; Ruiz-Martínez, A.; Robles, Á.; Serralta, J.; Ribes, J.; Rogalla, F.; Seco, A.; Ferrer, J. A semi-industrial AnMBR plant for urban wastewater treatment at ambient temperature: Analysis of the filtration process, energy balance and quantification of GHG emissions. *J. Environ. Chem. Eng.* **2023**, *11*, 109454. [CrossRef]

54. Italian Republic. Legislative Decree No. 152 of 3 April 2006 on Environmental Regulations (Environmental Code) 2006. Available online: https://www.normattiva.it/uri-res/N2Ls?urn:nir:stato:decreto.legislativo:2006-04-03;152 (accessed on 4 May 2025).

55. Directive (EU) 2024/1203 of the European Parliament and of the Council of 11 April 2024 on the Protection of the Environment Through Criminal Law and Replacing Directives 2008/99/EC and 2009/123/EC 2024. Available online: http://data.europa.eu/eli/dir/2024/1203/oj/eng (accessed on 4 May 2025).

56. Moral Pajares, E.; Gallego Valero, L.; Román Sánchez, I.M. Cost of Urban Wastewater Treatment and Ecotaxes: Evidence from Municipalities in Southern Europe. *Water* **2019**, *11*, 423. [CrossRef]

57. Annual Inflation Stable at 2.2% in the Euro Area. Available online: https://ec.europa.eu/eurostat/web/products-euro-indicators/w/2-19052025-ap (accessed on 28 May 2025).

58. U.S. Geological Survey (USGS). *Mineral Commodity Summaries 2025*; U.S. Geological Survey: Reston, VA, USA, 2025. Available online: https://pubs.usgs.gov/periodicals/mcs2025/mcs2025.pdf (accessed on 16 May 2025).

59. León, M.; Silva, J.; Carrasco, S.; Barrientos, N. Design, Cost Estimation and Sensitivity Analysis for a Production Process of Activated Carbon from Waste Nutshells by Physical Activation. *Processes* **2020**, *8*, 945. [CrossRef]

60. Yang, L.; Hao, C.; Chai, Y. Life Cycle Assessment of Commercial Delivery Trucks: Diesel, Plug-In Electric, and Battery-Swap Electric. *Sustainability* **2018**, *10*, 4547. [CrossRef]

61. Conflavoro PMI. CCNL Metalmeccanico Industria. National Collective Labour Agreement for the Metalworking Industry. Conflavoro PMI. 2021. Available online: https://file.conflavoro.it/pdf/ccnl/ccnl_metalmeccanico_industria_conflavoro.pdf (accessed on 1 June 2025).

62. Databases—AssessCCUS. Available online: https://assessccus.globalco2initiative.org/tea/databases/ (accessed on 28 May 2025).

63. European Central Bank. Official Interest Rates. Available online: https://www.ecb.europa.eu/stats/policy_and_exchange_rates/key_ecb_interest_rates/html/index.en.html (accessed on 28 May 2025).

64. Pipitone, G.; Zoppi, G.; Pirone, R.; Bensaid, S. Sustainable aviation fuel production using in-situ hydrogen supply via aqueous phase reforming: A tech-no-economic and life-cycle greenhouse gas emissions assessment. *J. Clean. Prod.* **2023**, *418*, 138141. [CrossRef]

65. Green, D.W.; Southard, M.Z. *Perry's Chemical Engineers' Handbook*, 9th ed.; McGraw-Hill Education: New York, NY, USA, 2019.

66. The Chemical Engineering Plant Cost Index®—Chemical Engineering. Available online: https://www.chemengonline.com/pci-home/ (accessed on 28 May 2025).

67. ARERA. Annual Report 2024. Activities Carried Out and Work Programmes. Italian Regulatory Authority for Energy, Networks and Environment, Vol. 1. 2024. Available online: https://www.arera.it/fileadmin/allegati/relaz_ann/24/RA24_vol1.pdf (accessed on 30 May 2025).

68. International Organization for Standardization (ISO). *Environmental Management—Life Cycle Assessment—Principles and Framework (ISO 14040:2006)*; International Organization for Standardization: Geneva, Switzerland, 2006.

69. International Organization for Standardization (ISO). *Environmental Management—Life Cycle Assessment—Requirements and Guidelines (ISO 14044:2006)*; ISO: Geneva, Switzerland, 2006.

70. Weidema, B.P.; Bauer, C.; Hischier, R.; Mutel, C.; Nemecek, T.; Reinhard, J.; Vadenbo, C.O.; Wernet, G. Overview and Methodology: Data Quality Guideline for the Ecoinvent Database Version 3. Swiss Centre for Life Cycle Inventories. Ecoinvent Report Vol. 3 No. 1. 2013. Available online: https://vbn.aau.dk/ws/portalfiles/portal/176769045/Overview_and_methodology.pdf (accessed on 30 May 2025).

71. Mutel, C. Brightway: An Open Source Framework for Life Cycle Assessment. *J. Open Source Softw.* **2024**, *2*, 236. [CrossRef]

72. Zampori, L.; Pant, R. Suggestions for Updating the Product Environmental Footprint (PEF) Method. JRC Publications Repository. Available online: https://publications.jrc.ec.europa.eu/repository/handle/JRC115959 (accessed on 4 June 2025).

73. Crenna, E.; Secchi, M.; Benini, L.; Sala, S. Global environmental impacts: Data sources and methodological choices for calculating normalization factors for LCA. *Int. J. Life Cycle Assess* **2019**, *24*, 1851–1877. [CrossRef]

74. Sala, S. Development of a Weighting Approach for the Environmental Footprint. JRC Publications Repository. Available online: https://publications.jrc.ec.europa.eu/repository/handle/JRC106545 (accessed on 4 June 2025).

75. Kolpakova, V.; Ospanov, K.; Kuldeyev, E.; Andraka, D. Clarification of Biologically Treated Wastewater in a Clarifier with Suspended Sludge Layer. *Water* **2021**, *13*, 2486. [CrossRef]

76. Seretis, A.; Tsiakaras, P. A thermodynamic analysis of hydrogen production via aqueous phase reforming of glycerol. *Fuel Process. Technol.* **2015**, *134*, 107–115. [CrossRef]

77. Coronado, I.; Stekrova, M.; Reinikainen, M.; Simell, P.; Lehtonen, J. A review of catalytic aqueous-phase reforming of oxygenated hydrocarbons derived from biorefinery water fractions. *Int. J. Hydrogen Energy* **2016**, *41*, 11003–11032. [CrossRef]

78. Towler, G.P.; Sinnott, R.K. *Chemical Engineering Design: Principles, Practice, and Economics of Plant and Process Design*, 2nd ed.; Butterworth-Heinemann: Boston, MA, USA, 2013.

79. Sutton, G.; Fateev, A.; Rodríguez-Conejo, M.A.; Meléndez, J.; Guarnizo, G. Validation of Emission Spectroscopy Gas Temperature Measurements Using a Standard Flame Traceable to the International Temperature Scale of 1990 (ITS-90). *Int. J. Thermophys.* **2019**, *40*, 99. [CrossRef]

80. Yang, H.; Jin, S.; He, Y.; Liu, Y. Experimental study on flame temperature distribution and pollutant emission characteristics of CH4 mixed with $CO_2/N2/H_2$ combustion. *Int. J. Hydrogen Energy* **2024**, *71*, 750–762. [CrossRef]

81. Nordio, M.; Wassie, S.A.; Van Sint Annaland, M.; Tanaka, D.A.P.; Sole, J.L.V.; Gallucci, F. Techno-economic evaluation on a hybrid technology for low hydrogen concentration separation and purification from natural gas grid. *Int. J. Hydrogen Energy* **2021**, *46*, 23417–23435. [CrossRef]

82. Salkuyeh, Y.K.; Saville, B.A.; MacLean, H.L. Techno-economic analysis and life cycle assessment of hydrogen production from natural gas using current and emerging technologies. *Int. J. Hydrogen Energy* **2017**, *42*, 18894–18909. [CrossRef]

83. Tribe, M.A.; Alpine, R.L.W. Scale economies and the "0.6 rule". *Eng. Costs Prod. Econ.* **1986**, *10*, 271–278. [CrossRef]

84. U.S. Environmental Protection Agency. *Catalog of CHP Technologies*, Washington, DC. 2015. Available online: https://www.epa.gov/sites/default/files/2015-07/documents/catalog_of_chp_technologies.pdf (accessed on 29 May 2025).

85. U.S. Department of Energy. Clean Hydrogen Production Cost Scenarios with PEM Electrolyzer Technology. DOE Hydrogen Program Record #24005, 20 May 2024. Available online: https://www.hydrogen.energy.gov/docs/hydrogenprogramlibraries/pdfs/24005-clean-hydrogen-production-cost-pem-electrolyzer.pdf?sfvrsn=8cb10889_1 (accessed on 29 May 2025).

86. Zheng, Z.; Lu, Z.; Tan, Q.; Yang, F.; Resasco, D. Synergistic bimetallic Ru–Pt catalysts for the low-temperature aqueous phase reforming of ethanol. *AIChE J.* **2019**, *65*, 151–160. [CrossRef]

87. Tito, E.; Zoppi, G.; Pipitone, G.; Miliotti, E.; Di Fraia, A.; Rizzo, A.M.; Pirone, R.; Chiaramonti, D.; Bensaid, S. Conceptual design and techno-economic assessment of coupled hydrothermal liquefaction and aqueous phase re-forming of lignocellulosic residues. *J. Environ. Chem. Eng.* **2023**, *11*, 109076. [CrossRef]

88. Le-Boulch, D.; Morisset, V.; Jobard, Z.; Burguburu, A.; Czyrnek-Delêtre, M.M. Life cycle assessment of nuclear power in France: EDF case study. *EPJ Nucl. Sci. Technol.* **2024**, *10*, 8. [CrossRef]

89. International Energy Agency (IEA). Italy—Countries & Regions. Available online: https://www.iea.org/countries/italy/energy-mix (accessed on 24 June 2025).

90. Valente, A.; Iribarren, D.; Dufour, J. Harmonised life-cycle global warming impact of renewable hydrogen. *J. Clean. Prod.* **2017**, *149*, 762–772. [CrossRef]

91. Critical Raw Materials—European Commission. Available online: https://single-market-economy.ec.europa.eu/sectors/raw-materials/areas-specific-interest/critical-raw-materials_en (accessed on 25 June 2025).

92. Roy, B.; Leclerc, C.A. Study of preparation method and oxidization/reduction effect on the performance of nickel-cerium oxide catalysts for aqueous-phase reforming of ethanol. *J. Power Sources* **2015**, *299*, 114–124. [CrossRef]

93. Roy, B.; Artyushkova, K.; Pham, H.N.; Li, L.; Datye, A.K.; Leclerc, C.A. Effect of preparation method on the performance of the Ni/Al_2O_3 catalysts for aqueous-phase reforming of ethanol: Part II—Characterization. *Int. J. Hydrogen Energy* **2012**, *37*, 18815–18826. [CrossRef]